AEDC-TR-73-166

NOV 2 1973
NOV 27 1973
JAN 2 7 1974

CALCULATION OF THE BOUNDARY-LAYER FLOW IN THE WINDWARD SYMMETRY PLANE OF A SPHERICALLY BLUNTED AXISYMMETRIC BODY AT ANGLE OF ATTACK, INCLUDING STREAMLINE-SWALLOWING EFFECTS

Arloe W. Mayne, Jr.

ARO, Inc.

October 1973

Approved for public release; distribution unlimited.

VON KÁRMÁN GAS DYNAMICS FACILITY
ARNOLD ENGINEERING DEVELOPMENT CENTER
AIR FORCE SYSTEMS COMMAND
ARNOLD AIR FORCE STATION, TENNESSEE

Property of U. S. Air Force
AEDC LIBRARY
F40600-71-C-0002

NOTICES

When U. S. Government drawings specifications, or other data are used for any purpose other than a definitely related Government procurement operation, the Government thereby incurs no responsibility nor any obligation whatsoever, and the fact that the Government may have formulated, furnished, or in any way supplied the said drawings, specifications, or other data, is not to be regarded by implication or otherwise, or in any manner licensing the holder or any other person or corporation, or conveying any rights or permission to manufacture, use, or sell any patented invention that may in any way be related thereto.

Qualified users may obtain copies of this report from the Defense Documentation Center.

References to named commercial products in this report are not to be considered in any sense as an endorsement of the product by the United States Air Force or the Government.

CALCULATION OF THE BOUNDARY-LAYER FLOW IN THE WINDWARD SYMMETRY PLANE OF A SPHERICALLY BLUNTED AXISYMMETRIC BODY AT ANGLE OF ATTACK, INCLUDING STREAMLINE-SWALLOWING EFFECTS

Arloe W. Mayne, Jr.
ARO, Inc.

Approved for public release; distribution unlimited.

FOREWORD

The work reported herein was conducted by the Arnold Engineering Development Center (AEDC), Air Force Systems Command (AFSC), under Program Element 65802F.

The results of research presented were obtained by ARO, Inc. (a subsidiary of Sverdrup & Parcel and Associates, Inc.), contract operator of AEDC, AFSC, Arnold Air Force Station, Tennessee. The research was conducted from September 1971 to December 1972 under ARO Project Nos. VW5206 and VF203, and the manuscript was submitted for publication on July 13, 1973.

Appreciation and acknowledgment are extended to Mr. A. Martellucci, Consultant, Aerothermodynamics Laboratory, Reentry and Environmental Systems Division, General Electric Company, Philadelphia, Pennsylvania, and to Mr. F. K. Hube, ARO, Inc., for providing the author with detailed tabulations of their experimental data. Sincere appreciation is also extended to Mr. E. O. Marchand, ARO, Inc., for performing the inviscid flow solutions used in this investigation.

This technical report has been reviewed and is approved.

ELTON R. THOMPSON
Research and Development
Division
Directorate of Technology

ROBERT O. DIETZ
Director of Technology

ABSTRACT

The three-dimensional compressible boundary-layer equations are presented in a general Crocco-variables form, and particularized to the windward symmetry plane of a spherically blunted axisymmetric body at incidence under hypersonic conditions. Through the use of an eddy transport coefficient hypothesis and a streamwise intermittency factor, both transitional and fully turbulent boundary layers may be treated, in addition to laminar boundary-layer flow. A scheme is presented for determining the outer-edge boundary conditions to be applied to the boundary-layer equations, based on a mass flow balance treatment of the boundary-layer entrainment of the inviscid flow. A finite-difference technique is described for solving the set of partial differential equation governing the boundary-layer flow, and for treating the streamline-swallowing phenomenon. The method of treating the problem is validated by the good agreement obtained between results from the present method and both experimental data and other methods of calculation. Comparisons with experimental data are shown for both laminar and turbulent flow under hypersonic conditions and include cases where streamline-swallowing effects are large and cases where crossflow influences should be strong.

CONTENTS

Page

ABSTRACT iii
NOMENCLATURE vi
I. INTRODUCTION 1
II. GOVERNING EQUATIONS
2.1 The Boundary-Layer Equations 3
2.2 Transport Laws 11
2.3 Boundary Conditions 14
2.4 Treatment of Streamline Swallowing 16
III. NUMERICAL SOLUTION METHOD
3.1 Stagnation Point Solution 21
3.2 Solution for the Spherical Nose Region 26
3.3 Solution for the Aft Body 30
3.4 Numerical Treatment of Streamline Swallowing 33
IV. RESULTS OF CALCULATIONS
4.1 Numerical Experiments 35
4.2 Comparisons with Experiment and Other Calculations 36
V. RESULTS AND DISCUSSION 42
REFERENCES 43

ILLUSTRATIONS

Figure

1. Streamline Swallowing on Blunt Axisymmetric Body at Zero Angle of Attack 2
2. Orthogonal Coordinate System and Velocity Components for Boundary-Layer Equations 3
3. Zones of Influence and Dependence 14
4. Streamline Swallowing, Showing Control Volume for Mass Balance in the Windward Symmetry Plane of an Axisymmetric Body at Angle of Attack 16
5. Simplified Flow Diagram for Solution at a General Station 19
6. Coordinate System 20
7. Typical Section of Finite-Difference Grid for $0 < \xi \leqslant \pi/2 - \alpha - \theta_c$ 28
8. Heat-Transfer and Skin Friction Distributions on a 9-deg Sphere-Cone at Mach 10.9 37
9. Velocity and Total Enthalpy Profiles at $\xi = 2.5$ on a 9-deg Sphere-Cone at Mach 10.9 37
10. Heat-Transfer Distribution on a 15-deg Sphere-Cone in a Mach 10.6 Flow at $\alpha = 10$ deg and Re = 1.1×10^5 38
11. Heat-Transfer Distribution on a 15-deg Sphere-Cone at $\alpha = 10$ deg in a Mach 10.6 Flow with Re = 3.75×10^4 38

Figure | Page

12. Heat-Transfer Distribution on a 7.2-deg Sphere-Cone in a Mach 8 Flow at α = 4 deg and Re = 34467 39
13. Comparisons of Computed and Measured Stanton Numbers at ξ = 11.9 on an 11-deg Sphere-Cone at Mach 8 as a Function of α at Re = 1.75 x 10^5 41
14. Comparisons of Computed and Measured Stanton Numbers at ξ = 7.5 on an 11-deg Sphere-Cone at Mach 8 as a Function of α at Re = 2.33 x 10^5 41
15. Comparisons of Computed and Measured Stanton Numbers at ξ = 9.3 on a 14-deg Sphere-Cone at Mach 8 as a Function of α at Re = 1.75 x 10^5 42

NOMENCLATURE

A,B,C	Terms in general forms of finite-difference equations
A*	Damping constant
AX(I), I=1,14	Terms involving body geometry and boundary data
C_{f_ξ}	Coefficient of skin friction in ξ direction
C_{f_η}	Coefficient of skin friction in η direction
C_p	Specific heat at constant pressure
G	Normalized η component of velocity
H	Total enthalpy
h	Static enthalpy
h_1, h_2, h_3	Metric coefficients corresponding to ξ, η, and ζ coordinates
J	Transformed ζ component of velocity
K	Molecular (laminar) conductivity
K_m	Mixing-length constant
k	Eddy (turbulent) conductivity
L	Reference length

ℓ_m	Mixing length
NSPH	Number of ξ grid lines on hemisphere
NZ	Number of mesh points in ζ direction
P,Q	Terms used in solution of finite-difference equations
p	Pressure
Pr	Prandtl number
R	Gas constant
r	Radius about axis of symmetry
R_n	Nose radius
Re	Reference Reynolds number
S	Distance along body surface
S_t, S_T	Values of S at beginning and end of transition region
St	Stanton number based on free-stream conditions
s	General length
T	Temperature
U	Velocity in freestream
u,v,w	Velocity components in ξ, η, and ζ directions
X	Dummy variable representing Φ, G, or θ
y	Distance normal to body surface
y_ℓ	Boundary-layer thickness in mixing length
Z	Function of ξ and η used to introduce similarity
α	Angle of attack
α_{X_i}, i=1,5	Terms appearing in general forms of governing equations

γ	Ratio of specific heats
$\Delta\zeta$	Finite-difference grid spacing in ζ direction
$\Delta\xi$	Finite-difference grid spacing in ξ direction
ζ	Coordinate normal to body surface
η	Lateral coordinate
θ	Total enthalpy ratio, H/H_e
θ_c	Body slope at nose-aft body tangency; cone half-angle for sphere-cone
λ	Dummy variable of integration or streamwise intermittency factor
λ_m	Mixing-length constant
μ	Coefficient of viscosity
ξ	Longitudinal coordinate
ρ	Mass density
Φ	Shear function

SUBSCRIPTS

e	Value at outer edge of boundary layer
ℓ	Laminar
n	ζ-grid point location
$s\ell$	Value on separating line in inviscid flowfield
T	Turbulent
w	Value at body surface
∞	Value in freestream

SPECIAL NOTATION

$(\overline{})$	Bar denotes dimensional quantity
$(\ )'$	Prime denotes fluctuating component
$(\sim)$	Tilde denotes time-average

SECTION I
INTRODUCTION

In the calculation of the boundary layer over a body in supersonic or hypersonic flow, the specification of the outer-edge boundary conditions to be applied to the boundary-layer equations is complicated by the fact that the local flow conditions along the outer edge of the boundary layer depend upon the inclination of the bow shock wave to the free-stream velocity at the point where the fluid at the outer edge of the boundary layer crossed the bow shock. This problem is often referred to as streamline swallowing, in reference to the entrainment by the boundary layer of the inviscid flow over a body. The problem of streamline swallowing by the boundary layer on blunt bodies in supersonic or hypersonic flow is one which has received considerable attention in the cases of both two-dimensional and axially symmetric flow, e.g., Ferri (Ref. 1), Mayne and Adams (Ref. 2), and Mayne and Dyer (Ref. 3). In addition to these two-dimensional and axisymmetric flow situations, the phenomenon of streamline swallowing by the boundary layer on a sharp axisymmetric body at angle of attack has been considered by Mayne (Ref. 4). In this latter case, the influence of streamline swallowing on boundary-layer calculations was through the entrainment by the boundary layer of the lateral flow around the body; the analytical treatment of this problem required the application and solution of the full three-dimensional boundary-layer equations.

Streamline swallowing also influences the calculation of the boundary-layer flow over blunt-nosed axisymmetric bodies at angle of attack as noted by Fannelop and Waldman (Ref. 5), and it is the treatment of this problem, for the flow in the windward plane of symmetry, which is the subject of the present report. The extension of this work to the flow over the remainder of the body can, in principle, be performed by the technique of Ref. 4, but such an extension is not a trivial effort.

For the case of flow over a two-dimensional blunt body or an axisymmetric blunt body at zero incidence, the streamline-swallowing phenomenon may be demonstrated by first considering that in the classical treatment of the associated boundary-layer calculation, the outer-edge conditions for the boundary-layer equations are taken to be the conditions at the body surface computed by assuming inviscid flow over the body. This is equivalent to assuming that all of the fluid along the outer edge of the boundary layer crossed the normal portion of the bow shock wave. In actuality, however, as the flow proceeds along the body, and the boundary layer entrains fluid, the portion of the flow which crossed the blunter forward part of the shock is "swallowed" by the boundary layer, as indicated in Fig. 1. The fluid along the outer edge of the boundary layer on the aft portion of the body will have passed through an oblique part of the shock wave and will be at a different state than had it passed through a normal shock wave. Naturally, the use of outer-edge conditions resulting from considering the streamline swallowing yields solutions to the boundary-layer equations which differ from those solutions obtained using the classical treatment of the outer-edge conditions. References 1, 2, 3, and 4 show significant effects of the streamline swallowing on computed boundary-layer profile data, surface heat-transfer rate, and skin friction.

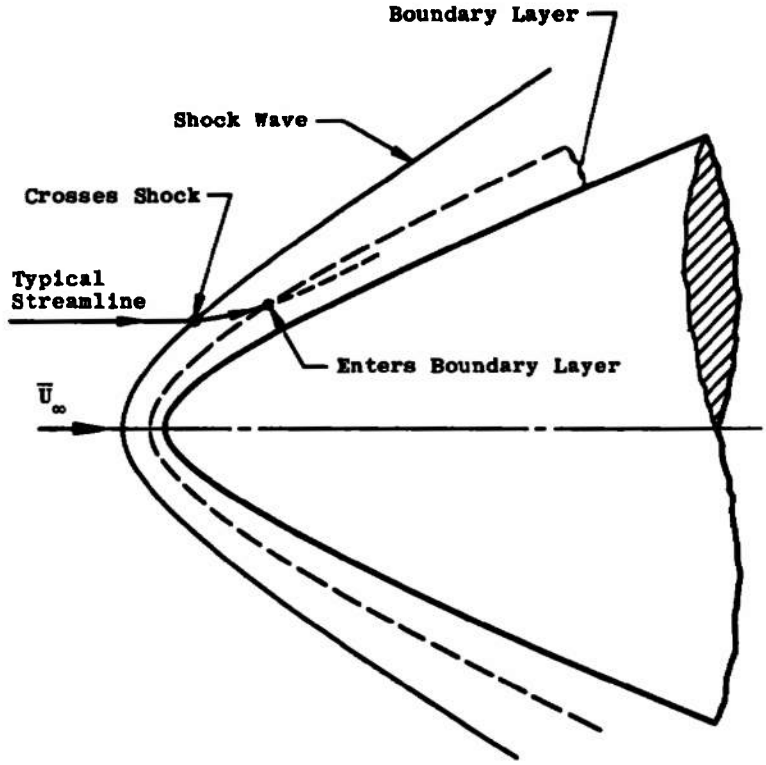

Fig. 1 Streamline Swallowing on Blunt Axisymmetric Body at Zero Angle of Attack

For the case of a blunt axisymmetric body at incidence, the streamline-swallowing phenomenon is basically the same as that for the body at zero incidence. However, because of the existence of crossflow in both the boundary layer and in the inviscid flow, the relatively simple global mass-balance treatment of the streamline swallowing which can be used in the zero incidence treatment (as in Ref. 2, for example) must be replaced by a local mass balance between the boundary-layer flow and the inviscid flow when streamline swallowing is to be considered on a body at incidence. In the work reported herein, this has been accomplished through particularizing the streamline-swallowing treatment of Ref. 4 to the windward plane of symmetry of a spherically blunted axisymmetric body at incidence. The governing equations are presented for the case of an arbitrary spherically blunted axisymmetric body, and results are presented showing the effects of streamline swallowing on windward-plane-of-symmetry solutions to the three-dimensional boundary-layer equations for cases of hypersonic flow over spherically blunted right circular cones at angle of attack. Using the eddy viscosity-intermittency factor approach described by Adams (Ref. 6), laminar, transitional, and turbulent boundary-layer flows are treated.

SECTION II
GOVERNING EQUATIONS

In this section are presented the governing equations for three-dimensional compressible boundary-layer flow and a discussion of the boundary conditions required to solve the equations, including their determination through the consideration of the streamline-swallowing phenomenon. The boundary-layer equations are presented in a Crocco-variables form which is the same as that used in Ref. 4 except that in the present work the Prandtl number is not required to be a constant. (A variable Prandtl number is permitted in order to allow the consideration of turbulent boundary layers through an eddy-transport concept.) In order to permit their application to any desired body, the equations presented in this section are not based on a particular body geometry.

The gas under consideration is assumed to be both thermally and calorically perfect. The governing partial differential equations for three-dimensional compressible boundary-layer flow (given by Mager (Ref. 7), for example) are the continuity equation, a longitudinal momentum equation, a lateral momentum equation, and an energy equation. The Crocco transformation is used to eliminate the component of velocity normal to the body surface as a dependent variable and, thereby, to reduce the number of partial differential equations which must be solved from four to three.

2.1 THE BOUNDARY-LAYER EQUATIONS

The boundary-layer equations are given in the orthogonal (ξ, η, ζ) coordinate system indicated in Fig. 2, where ξ and η are orthogonal coordinates defined in the surface over which the boundary layer flows. The coordinate ζ is normal to the body surface; in this report $\zeta = 0$ on the body surface. The symbols u, v, and w represent the nondimensional velocity components in the ξ, η, and ζ directions, respectively. For this coordinate system the general element of length is

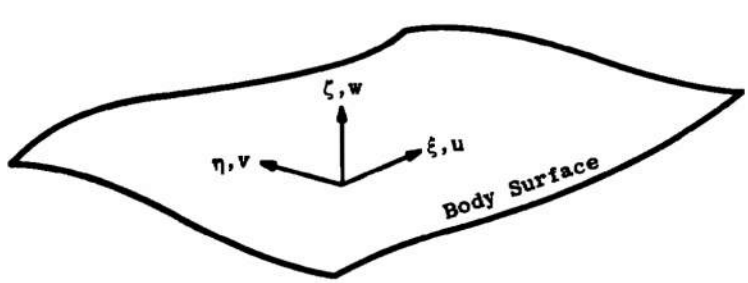

Fig. 2 Orthogonal Coordinate System and Velocity Components for Boundary-Layer Equations

$$(d\bar{s})^2 = \bar{h}_1^{\,2}\,(d\xi)^2 + \bar{h}_2^{\,2}\,(d\eta)^2 + \bar{h}_3^{\,2}\,(d\zeta)^2 \tag{1}$$

where a bar over a quantity denotes a dimensional quantity. It is assumed that $\overline{h_1}$ and $\overline{h_2}$ are functions of only ξ and η; this is equivalent to neglecting transverse curvature in axisymmetric boundary-layer flow. The metric coefficient $\overline{h_3}$ is a function of ξ, η, and ζ; $\overline{h_3}\ d\zeta$ is a differential element of the physical distance normal to the body surface, i.e., $\overline{h_3}\ d\zeta = d\overline{y}$.

The variables in the boundary-layer equations are nondimensionalized according to the following scheme:

$$h_1 = \frac{\overline{h_1}}{\overline{L}} \qquad \mu = \frac{\overline{\mu}}{\overline{\mu}_\infty}$$

$$h_2 = \frac{\overline{h_2}}{\overline{L}} \qquad p = \frac{\overline{p}}{\overline{\rho}_\infty\ \overline{U}_\infty^{\,2}}$$

$$h_3 = \frac{\overline{h_3}\ \sqrt{Re}}{\overline{L}} \qquad \rho = \frac{\overline{\rho}}{\overline{\rho}_\infty}$$

$$u = \frac{\overline{u}}{\overline{U}_\infty} \qquad T = \frac{\overline{T}\ \overline{c}_p}{\overline{U}_\infty^{\,2}}$$

$$v = \frac{\overline{v}}{\overline{U}_\infty} \qquad H = \frac{\overline{H}}{\overline{U}_\infty^{\,2}}$$

$$w = \frac{\overline{w}\ \sqrt{Re}}{\overline{U}_\infty} \tag{2}$$

where

$$Re = \frac{\overline{\rho}_\infty\ \overline{U}_\infty\ \overline{L}}{\overline{\mu}_\infty} \tag{3}$$

The Reynolds number factor appearing in the relations for h_3 and w is not necessary to nondimensionalize these variables; however, it does serve to eliminate any explicit dependence of the resulting equations on the free-stream Reynolds number.

The Crocco transformation is accomplished by letting the coordinate normal to the body surface be defined to be the longitudinal velocity component, or, in the present treatment, a normalized form of the longitudinal velocity. This yields the convenient limits of zero and unity for the normal coordinate. (The term "longitudinal" is used to refer to the ξ direction, and "lateral" is used to refer to the η direction. The term "normal" refers, of course, to the ζ direction.) The velocity component normal to the body surface is eliminated from the equations by combining the longitudinal momentum equation with each of the continuity, lateral momentum, and energy equations. This results in eliminating one of the partial differential equations entirely. As a part of the transformation, a form of the longitudinal component of the shearing stress becomes the dependent variable associated with the transformed longitudinal momentum equation.

The Crocco transformation is accomplished by first introducing the following definitions:

$$\zeta = \frac{u}{u_e} \qquad G = \frac{v}{v_e}$$

$$J = \frac{wZ}{u_e} \qquad \theta = \frac{H}{H_e} \tag{4}$$

$$\Phi = \frac{\mu Z}{h_3}$$

where Z is a function of ξ and η which can be defined for a particular case so as to eliminate singularities at a stagnation point or sharp tip of a body, or to introduce similarity into certain cases. The subscript "e" refers to the value of a variable at the outer edge of the boundary layer; quantities so designated are functions of only ξ and η. In order for the Crocco transformation to be meaningful, it is necessary that u increase monotonically from zero at the body surface to u_e at the outer edge of the boundary layer.

The independent variables in the transformed equations are ξ, η, and $\zeta = u/u_e$. The dependent variables associated with the transformed differential equations are G, J, θ, and Φ, although J is eliminated from the equations. The usual assumption is made of a constant pressure across the boundary layer, i.e., $\partial p/\partial \zeta = 0$. Through the definitions of the coordinate ζ and the metric coefficient h_3, Φ is proportional to the longitudinal component of the shearing stress.

The nondimensional temperature may be expressed as

$$T = H_e\,\theta - \frac{1}{2}\left(\zeta^2 u_e^2 + G^2 v_e^2\right) \tag{5}$$

For convenience the temperature is retained in the transformed differential equations, although it is an explicit function of the edge conditions and the primary dependent variables. The nondimensional viscosity is treated similarly.

The application of the transformations given by Eq. (4) to the ξ-momentum equation permits the determination of the following expression for J, the transformed velocity component normal to the body surface:

$$
\begin{aligned}
J = {} & \frac{\gamma-1}{\gamma}\,\frac{1}{u_e}\,\frac{T}{p}\,\frac{\partial\Phi}{\partial\zeta} - \frac{\gamma-1}{\gamma}\,\frac{\mu Z^2}{u_e^2\,\Phi}\,\frac{T}{p h_1}\,\frac{\partial p}{\partial\xi} \\
& - \frac{\mu Z^2\,\zeta^2}{u_e \Phi\, h_1}\,\frac{\partial u_e}{\partial\xi} - \frac{\mu Z^2\, v_e\,\zeta\, G}{u_e\,\Phi\, h_2}\,\frac{\partial \ln\,(u_e h_1)}{\partial\eta} \\
& + \frac{\mu Z^2\, v_e^2\, G^2}{u_e^2\,\Phi\, h_1 h_2}\,\frac{\partial h_2}{\partial\xi}
\end{aligned}
\tag{6}
$$

The use of Eq. (6) to eliminate the velocity component normal to the body surface from the continuity equation yields the following equation, which may be considered to be the Crocco-variables form of the ζ-momentum equation:

$$
\frac{\partial^2\Phi}{\partial\zeta^2} + \alpha_{\Phi 1}\,\frac{\partial\Phi}{\partial\zeta} + \alpha_{\Phi 2}\;\Phi + \alpha_{\Phi 3} + \alpha_{\Phi 4}\,\frac{\partial\Phi}{\partial\xi} + \alpha_{\Phi 5}\,\frac{\partial\Phi}{\partial\eta} = 0 \tag{7}
$$

where

$$
\alpha_{\Phi 1} = AX(5)\,\frac{\mu\zeta^2}{\Phi^2 T} + AX(6)\,\frac{\mu\zeta G}{\Phi^2 T} - AX(7)\,\frac{\mu G^2}{\Phi^2 T} + AX(8)\,\frac{\mu}{\Phi^2}
$$

$$
\alpha_{\Phi 2} = 0
$$

$$
\begin{aligned}
\alpha_{\Phi 3} = \frac{\mu}{\Phi T}\Bigg\{ & AX(1)\,\frac{\zeta}{\mu}\,\frac{\partial\mu}{\partial\xi} - AX(1)\,\frac{\zeta}{T}\,\frac{\partial T}{\partial\xi} \\
& + AX(2)\,\frac{\partial G}{\partial\eta} + AX(2)\,\frac{G}{\mu}\,\frac{\partial\mu}{\partial\eta} - AX(2)\,\frac{G}{T}\,\frac{\partial T}{\partial\eta} \\
& + AX(3)\zeta + AX(4)G - AX(5)2\zeta - AX(5)\,\frac{\zeta^2}{\mu}\,\frac{\partial\mu}{\partial\zeta} \\
& + AX(5)\,\frac{\zeta^2}{T}\,\frac{\partial T}{\partial\zeta} - AX(6)\zeta\,\frac{\partial G}{\partial\zeta} - AX(6)G
\end{aligned}
$$

$$- AX(6)\frac{\zeta G}{\mu}\frac{\partial\mu}{\partial\zeta} + AX(6)\frac{\zeta G}{T}\frac{\partial T}{\partial\zeta} + AX(7)2G\frac{\partial G}{\partial\zeta}$$

$$\left. + AX(7)\frac{G^2}{\mu}\frac{\partial\mu}{\partial\zeta} - AX(7)\frac{G^2}{T}\frac{\partial T}{\partial\zeta} - AX(8)\frac{T}{\mu}\frac{\partial\mu}{\partial\zeta}\right\}$$

$$\alpha_{\phi 4} = - AX(1)\frac{\mu\zeta}{\phi^2 T}$$

$$\alpha_{\phi 5} = - AX(2)\frac{\mu G}{\phi^2 T} \tag{8}$$

Equation (7) is cast into a standard form which is convenient for the numerical solution technique presented in Section III. The AX(I) coefficients in Eq. (8) are functions of the body geometry and the outer-edge conditions. Since many of them occur a number of times, their explicit forms are given later in this section.

The η-momentum equation expressed in Crocco variables form is

$$\frac{\partial^2 G}{\partial\zeta^2} + \alpha_{G1}\frac{\partial G}{\partial\zeta} + \alpha_{G2}\, G + \alpha_{G3} + \alpha_{G4}\frac{\partial G}{\partial\xi} + \alpha_{G5}\frac{\partial G}{\partial\eta} = 0 \tag{9}$$

where

$$\alpha_{G1} = AX(5)\frac{\mu}{\phi^2 T}\zeta^2 + AX(6)\frac{\mu\zeta G}{\phi^2 T} - AX(7)\frac{\mu G^2}{\phi^2 T} + AX(8)\frac{\mu}{\phi^2}$$

$$\alpha_{G2} = -AX(10)\frac{\mu\zeta}{\phi^2 T} - AX(11)\frac{\mu G}{\phi^2 T}$$

$$\alpha_{G3} = AX(9)\frac{\mu\zeta^2}{\phi^2 T} - AX(12)\frac{\mu}{\phi^2}$$

$$\alpha_{G4} = - AX(1)\frac{\mu\zeta}{\phi^2 T}$$

$$\alpha_{G5} = - AX(2)\frac{\mu G}{\phi^2 T} \tag{10}$$

The Crocco variables form of the energy equation, for variable Prandtl number, is

$$\frac{\partial^2\theta}{\partial\zeta^2} + \alpha_{\theta 1}\frac{\partial\theta}{\partial\zeta} + \alpha_{\theta 2}\theta + \alpha_{\theta 3} + \alpha_{\theta 4}\frac{\partial\theta}{\partial\xi} + \alpha_{\theta 5}\frac{\partial\theta}{\partial\eta} = 0 \tag{11}$$

where

$$\alpha_{\theta 1} = \frac{(1-Pr)}{\Phi}\frac{\partial\Phi}{\partial\zeta} + AX(5)\frac{\mu Pr\zeta^2}{\Phi^2 T} + AX(6)\frac{\mu Pr\zeta G}{\Phi^2 T}$$

$$- AX(7)\frac{\mu PrG^2}{\Phi^2 T} + AX(8)\frac{\mu Pr}{\Phi^2} - \frac{1}{Pr}\frac{\partial Pr}{\partial\zeta}$$

$$\alpha_{\theta 2} = 0$$

$$\alpha_{\theta 3} = - AX(13)(1-Pr)\left(1 + \frac{\zeta}{\Phi}\frac{\partial\Phi}{\partial\zeta}\right) + AX(13)\frac{\zeta}{Pr}\frac{\partial Pr}{\partial\zeta}$$

$$- AX(14)(1-Pr)\left[\frac{G}{\Phi}\frac{\partial G}{\partial\zeta}\frac{\partial\Phi}{\partial\zeta} + G\left(\frac{\partial^2 G}{\partial\zeta^2}\right) + \left(\frac{\partial G}{\partial\zeta}\right)^2\right]$$

$$+ AX(14)\frac{G}{Pr}\frac{\partial G}{\partial\zeta}\frac{\partial Pr}{\partial\zeta}$$

$$\alpha_{\theta 4} = - AX(1)\frac{\mu Pr\zeta}{\Phi^2 T}$$

$$\alpha_{\theta 5} = - AX(2)\frac{\mu PrG}{\Phi^2 T} \tag{12}$$

Although the grouping of some of the η-momentum equation coefficients of Eqs. (9) and (10) is not unique, they have been formulated analogous to the coefficients for the ξ-momentum and energy equations, and the groupings presented have proven well-behaved in the solution of the equations.

While performing the Crocco transformation, the density was eliminated from the equations through the use of the perfect gas equation of state and the relationship $\overline{R} = (\gamma-1)/\gamma\ \overline{C}_p$.

The coefficients AX(1) through AX(14) are functions of only ξ and η, and not ζ. They are essentially made up of body geometry data and data concerning conditions along the outer edge of the boundary layer. Their explicit forms are

$$AX(1) = \frac{\gamma}{\gamma-1} \frac{u_e p Z^2}{h_1}$$

$$AX(2) = \frac{\gamma}{\gamma-1} \frac{v_e p Z^2}{h_2}$$

$$AX(3) = \frac{\gamma}{\gamma-1} \frac{Z}{h_1 h_2} \frac{\partial}{\partial \xi} \quad (h_2 Z p u_e)$$

$$AX(4) = \frac{\gamma}{\gamma-1} \frac{Z}{h_1 h_2} \frac{\partial}{\partial \eta} \quad (h_1 Z p v_e)$$

$$AX(5) = \frac{\gamma}{\gamma-1} \frac{p Z^2}{h_1} \frac{\partial u_e}{\partial \xi}$$

$$AX(6) = \frac{\gamma}{\gamma-1} \frac{v_e p Z^2}{h_2} \frac{\partial \ln(u_e h_1)}{\partial \eta}$$

$$AX(7) = \frac{\gamma}{\gamma-1} \frac{v_e^2 p Z^2}{u_e h_1 h_2} \frac{\partial h_2}{\partial \xi}$$

$$AX(8) = \frac{Z^2}{h_1 u_e} \frac{\partial p}{\partial \xi}$$

$$AX(9) = \frac{\gamma}{\gamma-1} \frac{u_e^2 p Z^2}{v_e h_1 h_2} \frac{\partial h_1}{\partial \eta}$$

$$AX(10) = \frac{\gamma}{\gamma-1} \frac{u_e p Z^2}{h_1} \frac{\partial \ln(v_e h_2)}{\partial \xi}$$

$$AX(11) = \frac{\gamma}{\gamma-1} \frac{p Z^2}{h_2} \frac{\partial v_e}{\partial \eta}$$

$$AX(12) = \frac{Z^2}{v_e h_2} \frac{\partial p}{\partial \eta}$$

$$AX(13) = \frac{u_e^2}{He}$$

$$AX(14) = \frac{v_e^2}{He} \tag{13}$$

In utilizing the results of calculations performed using the Crocco-variables form of the three-dimensional boundary-layer equations presented in this section, certain parameters are of interest from a physical standpoint. The coefficient of longitudinal skin friction may be obtained in the form

$$C_{f_\xi} Z \sqrt{Re} = 2 u_e(\Phi)_{\zeta=0} \tag{14}$$

where

$$C_{f_\xi} = \frac{\left(\bar{\mu} \frac{\partial \bar{u}}{\partial \bar{y}}\right)_{\zeta=0}}{\frac{1}{2} \bar{\rho}_\infty \bar{U}_\infty^2}$$

The coefficient of lateral skin friction can be obtained as

$$C_{f_\eta} Z \sqrt{Re} = 2v_e \left(\Phi \frac{\partial G}{\partial \zeta}\right)_{\zeta=0} \tag{15}$$

where

$$C_{f_\eta} = \frac{\left(\bar{\mu} \frac{\partial \bar{v}}{\partial \bar{y}}\right)_{\zeta=0}}{\frac{1}{2} \bar{\rho}_\infty \bar{U}_\infty^2}$$

The Stanton number may be represented as

$$St_\infty Z \sqrt{Re} = \left[\frac{-\Phi}{Pr\ He(1-\theta)} \frac{\partial T}{\partial \zeta}\right]_{\zeta=0} \tag{16}$$

where

$$St_\infty = \frac{\left(\frac{\bar{\mu}\ \bar{C}_p}{Pr} \frac{\partial \bar{T}}{\partial \bar{y}}\right)_{\zeta=0}}{\bar{\rho}_\infty \bar{U}_\infty (\bar{H}_e - \bar{H}_{\zeta=0})}$$

The distance normal to the surface may be determined from

$$\frac{\bar{y} \sqrt{Re}}{\bar{L} Z} = \int_0^\zeta \frac{\mu}{\Phi} d\zeta \tag{17}$$

2.2 TRANSPORT LAWS

Equations (7), (9), and (11) are applicable to both laminar and turbulent boundary-layer flow if the viscosity and Prandtl number in the equations are considered to be "effective" transport parameters. The boundary-layer equations as given by Eqs. (7), (9), and (11) are equivalent to an eddy-exchange coefficient treatment of the Reynolds-averaged boundary-layer equations for turbulent flow (i.e., time-averaging of the equations where each dependent variable is expressed as the sum of a steady and a fluctuating component); more specifically, a scalar eddy viscosity is indicated by Eqs. (7), (9), and (11). The hypotheses leading to the forms of the transport terms in Eqs. (7), (9), and (11), for turbulent flows, are:

Shearing Stress Terms

$$\bar{\mu} \frac{\partial \bar{u}}{\partial \bar{y}} = \bar{\mu}_\ell \frac{\partial \bar{u}}{\partial \bar{y}} + \bar{\mu}_{T_\xi} \frac{\partial \bar{u}}{\partial \bar{y}}$$

$$\bar{\mu} \frac{\partial \bar{v}}{\partial \bar{y}} = \bar{\mu}_\ell \frac{\partial \bar{v}}{\partial \bar{y}} + \bar{\mu}_{T_\eta} \frac{\partial \bar{v}}{\partial \bar{y}}$$

and

$$\bar{\mu}_{T_\xi} = \bar{\mu}_{T_\eta} = \bar{\mu}_T$$

where

$$\bar{\mu}_{T_\xi} \frac{\partial \bar{u}}{\partial \bar{y}} = - \bar{\rho} \, \widetilde{u' w'}$$

$$\bar{\mu}_{T_\eta} \frac{\partial \bar{v}}{\partial \bar{y}} = - \bar{\rho} \, \widetilde{v' w'} \tag{18}$$

Energy Flux Terms

$$\bar{\mu} \left[\frac{1}{Pr} \frac{\partial \bar{h}}{\partial \bar{y}} + \frac{\partial}{\partial \bar{y}} \left(\frac{\bar{u}^2 + \bar{v}^2}{2} \right) \right]$$

$$= \left(\frac{\bar{K}}{\bar{C}_p} + \frac{\bar{k}}{\bar{C}_p} \right) \frac{\partial \bar{h}}{\partial \bar{y}} + (\bar{\mu}_\ell + \bar{\mu}_T) \frac{\partial}{\partial \bar{y}} \frac{\bar{u}^2 + \bar{v}^2}{2}$$

where

$$\frac{\bar{k}}{\bar{C}_p} \frac{\partial \bar{h}}{\partial \bar{y}} = - \bar{\rho} \, \widetilde{w' h'} \tag{19}$$

In Eqs. (18) and (19) the prime superscript refers to the fluctuating component of a variable, and the tilde refers to a time-average of a fluctuating quantity (quantities not otherwise indicated are time-averaged values). From Eqs. (18) and (19) the effective transport properties for momentum and energy may be seen to be

$$\bar{\mu} = \bar{\mu}_\ell + \bar{\mu}_T$$

$$\frac{\bar{\mu}}{\bar{Pr}} = \frac{\bar{K}}{\bar{C}_p} + \frac{\bar{k}}{\bar{C}_p}$$

or

$$\frac{\bar{\mu}}{\bar{Pr}} = \frac{\mu_\ell}{Pr_\ell} + \frac{\mu_T}{Pr_T}$$

where

$$Pr_T = \frac{\bar{\mu}_T \bar{C}_p}{\bar{k}} \tag{20}$$

In the present work the turbulent Prandtl number was assumed to be constant at a value of 0.9, and the laminar Prandtl number was assumed to be 0.7. The laminar viscosity was obtained using Sutherland's law.

The specification of the turbulent viscosity has been done using the mixing-length, invariant-turbulence model as applied by Adams (Ref. 6) and Hunt, Bushnell, and Beckwith (Ref. 8)

$$\bar{\mu}_T = \bar{\rho}\, \bar{\ell}_m^{\,2} \left[\left(\frac{\partial \bar{u}}{\partial \bar{y}} \right)^2 + \left(\frac{\partial \bar{v}}{\partial \bar{y}} \right)^2 \right]^{1/2} \tag{21}$$

The mixing length, $\bar{\ell}_m$, was obtained using a two-layer model, with exponential damping near the wall as recommended by van Driest (Ref. 9). The variation of $\bar{\ell}_m$ was obtained from the recommendations of Patankar and Spalding (Ref. 10) as

$$\bar{\ell}_m = K_m \bar{y} \left[1 - \exp\left(\frac{-\bar{y} \sqrt{\bar{\tau}\, \bar{\rho}}}{\bar{\mu} A^*} \right) \right]$$

for

$$0 < \bar{y} \leq \lambda_m \bar{y}_\ell / K_m$$

and

$$\bar{\ell}_m = \lambda_m \bar{y}_\ell$$

for

$$\lambda_m \bar{y}_\ell / K_m < \bar{y} \tag{22}$$

with $\bar{\tau}$, $\bar{\rho}$, and $\bar{\mu}$ evaluated at local conditions in the boundary layer.

The values used for K_m, A^*, and λ_m were 0.435, 26.0, and 0.09, respectively. The value of $\bar{y}$ at the point in the boundary layer where the velocity was 0.99 of the outer-edge velocity was used to define $\bar{y}_\ell$.

In order to treat boundary layers undergoing transition from laminar to turbulent flow, an intermittency factor, λ, was introduced into Eq. (20) to give

$$\bar{\mu} = \bar{\mu}_\ell + \lambda \bar{\mu}_T$$

$$\frac{\bar{\mu}}{Pr} = \frac{\bar{K}}{\bar{C}_p} + \lambda \frac{\bar{k}}{\bar{C}_p}$$

or

$$\frac{\bar{\mu}}{Pr} = \frac{\bar{\mu}_\ell}{Pr_\ell} + \lambda \frac{\bar{\mu}_T}{Pr_T} \tag{23}$$

The intermittency factor is the fraction of the time that the boundary layer is turbulent at a given location; λ is zero for laminar flow and one for fully turbulent flow. In the present investigation, the intermittency-factor distribution determined by Dhawan and Narasimha (Ref. 11) was used; this has the form

$$\lambda = 1 - \exp\left[-3.507\left(\frac{\bar{S} - \bar{S}_t}{\bar{S}_T - \bar{S}_t}\right)^2\right]$$

where $\bar{S}$ represents the distance along the body surface, $\bar{S}_t$ is the distance to the beginning of transition, and $\bar{S}_T$ is the distance to the end of transition. In order to use this form of the intermittency-factor distribution, it is necessary to let λ be somewhat less than unity at $\bar{S} = \bar{S}_T$; in the form given, it is assumed that $\lambda = 0.97$ at $\bar{S} = \bar{S}_T$.

In the calculations made in this investigation, no attempt was made to compute or predict the locations of the beginning and end of transition; instead, experimental data were used to specify $\bar{S}_t$ and $\bar{S}_T$ for each case considered.

2.3 BOUNDARY CONDITIONS

The appropriate boundary conditions necessary to solve the set composed of Eqs. (7), (9), and (11) depend upon the nature of the equations. This matter has been considered in detail by Raetz (Ref. 12), Der and Raetz (Ref. 13), and Wang (Ref. 14). In considering the situation for a general point P in the boundary layer, the concept of zones of influence and dependence have been developed as illustrated in Fig. 3. The partial differential equations are of an elliptic nature in the ζ direction, and the conditions at point P affect, and are in turn affected by, the conditions along the entire line which is normal to the surface from $\zeta = 0$ to $\zeta = 1$ and passes through P. This elliptical nature is due to the diffusion phenomena which occur. Downstream of P there is a zone of influence bounded by the surfaces called the "outer and inner characteristic envelopes". These characteristic envelopes are generated by the normals to the surface emanating from the projection on the surface of the streamlines having either the minimum or maximum angular displacement from constant-η surfaces. The conditions at point P affect the conditions at all points within this zone of influence. Upstream of P there exists a similarly defined zone of dependence such that the conditions at P are dependent upon the conditions at all points within the zone of dependence.

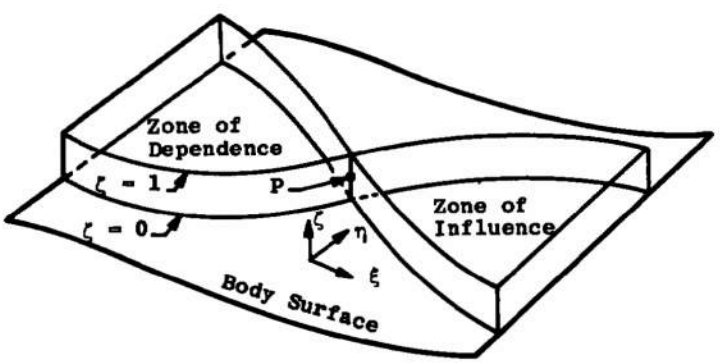

Fig. 3 Zones of Influence and Dependence

Raetz's influence principle, based upon the concept of zones of dependence and influence, is essential in determining the appropriate boundary conditions and even a solution technique for solving general three-dimensional boundary-layer problems. Application of this principle is discussed in Refs. 4, 12, and 13. For the present problem of flow in the windward symmetry plane of a spherically blunted axisymmetric body, the governing equations degenerate to a two-point boundary-value problem at the stagnation point and to a two-dimensional parabolic system for the remainder of the windward symmetry plane. (The zones of dependence and influence degenerate to sections of the windward symmetry plane.) Were the boundary-layer flow to be computed over the entire axisymmetric body the windward symmetry plane results of this investigation would be necessary to continue the solution of the governing equations over the remainder of the body.

In general, the boundary conditions to be imposed on G and θ at the body surface (ζ = 0) and at the outer edge of the boundary layer (ζ = 1) are:

$$\text{at } \underline{\zeta = 0}: \qquad G = 0$$

$$\theta = [\theta(\xi,\eta)]_{\zeta=0}, \text{ prescribed}$$

$$\text{at } \underline{\zeta = 1}: \qquad G = 1 \tag{24}$$

$$\theta = 1$$

The surface boundary condition on θ could also be the equivalent of a prescribed heat-transfer-rate distribution, although that possibility is not treated herein.

The surface boundary condition on Φ is obtained from evaluating Eq. (6), the Crocco-variables form of the ξ-momentum equation, at ζ = 0, where G is also zero. The resulting expression yields

$$\left(\frac{\partial\Phi}{\partial\zeta}\right)_{\zeta=0} = \left[\frac{\gamma}{\gamma-1}\,\frac{u_e\,pJ}{T} + AX(8)\,\frac{\mu}{\Phi}\right]_{\zeta=0} \tag{25}$$

The factor J in Eq. (25) would be used to include surface mass transfer effects if transpiration or suction were being considered.

The outer-edge boundary condition on Φ may be obtained from the definition of Φ as

$$(\Phi)_{\zeta=1.0} = \left(\frac{\mu\,Z}{\sqrt{Re}\,u_e}\,\frac{du}{dy}\right)_{\zeta=1.0} \tag{26}$$

where

$$y = \frac{\bar{y}}{\bar{L}}$$

In the classical treatment of boundary-layer theory, the term $(du/dy)_{\zeta=1.0}$ is set equal to zero. In the present treatment of the problem, however, where streamline swallowing is being considered, this term is equated to its value at a certain point in the inviscid flowfield. It should also be noted that u_e, v_e, and their variation with ξ and η must also be determined in an appropriate manner from the inviscid flowfield over the body. This matter is considered in the next section.

2.4 TREATMENT OF STREAMLINE SWALLOWING

In this subsection, the technique used to determine the boundary-layer outer-edge conditions through the treatment of the streamline-swallowing phenomenon is presented. Basically, the boundary-layer outer-edge conditions are determined on a line in the windward symmetry plane of the inviscid flow field which separates the flow entrained by the boundary layer from that not entrained by the boundary layer. The location of this line in the inviscid flow field is obtained by means of a mass balance between the boundary layer and the inviscid flow field. In the actual computations, the location of this line is coupled to the solution of the boundary-layer equations and is obtained in an iterative manner in conjunction with the solution of the boundary-layer equations. It is assumed herein that boundary-layer displacement effects on the inviscid flow field are negligible, and no such effects have been considered in this investigation. Also, it is assumed that there is no surface mass transfer; consideration of surface mass transfer would require modifications to the scheme described in this subsection.

In Ref. 4 a general method was described for determining the boundary-layer outer-edge conditions when considering streamline swallowing in a three-dimensional flow situation. The present scheme is equivalent to specializing the method of Ref. 4 to the flow in the windward symmetry plane of an axisymmetric body at angle of attack. A description of the method of determining the location of the separating line discussed in the previous paragraph can be accomplished by anticipating the finite-difference treatment used in the solution of the associated boundary-layer problem. The description of the method of determining the location of the separating line in the inviscid flow field is, therefore, done from a control-volume point of view which is analogous to the finite-difference treatment of the boundary-layer problem.

The basic relationship used to find the location of the line in the inviscid flow field which separates the flow entrained by the boundary layer from that not entrained by the boundary layer can be given in terms of the sketch shown in Fig. 4. If that part

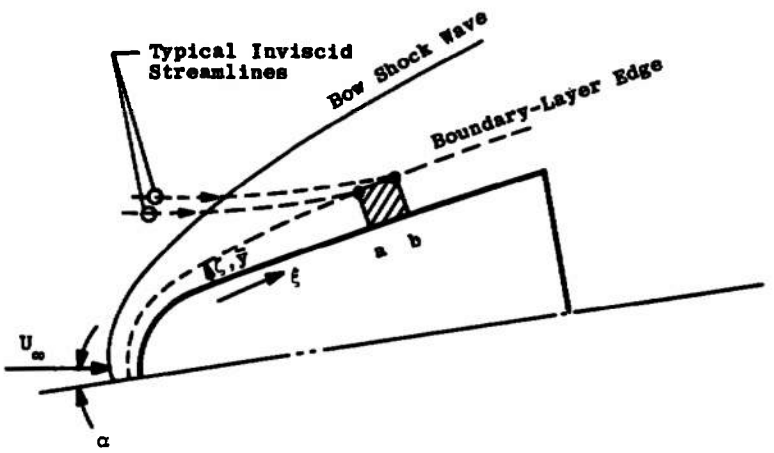

Fig. 4 Streamline Swallowing, Showing Control Volume for Mass Balance in the Windward Symmetry Plane of an Axisymmetric Body at Angle of Attack

of the inviscid flow which crosses the separating line between locations a and b is equated to the flow which enters the boundary layer between locations a and b, the following equation results:

$$\int_{\xi_a}^{\xi_b}\int_0^1 \bar{\rho}' \frac{\partial \bar{v}'}{\partial \eta} \bar{h}_3 d\zeta\, \bar{h}_1 d\xi + \left[\bar{h}_2 \int_0^1 \bar{\rho}'\, \bar{u}'\, \bar{h}_3\, d\zeta\right]_{\xi=\xi_b}$$

$$- \left[\bar{h}_2 \int_0^1 \bar{\rho}'\, \bar{u}'\, \bar{h}_3\, d\zeta\right]_{\xi=\xi_a} = \left[\bar{h}_2 \int_0^{\bar{y}_{s\ell}} \bar{\rho}^*\, \bar{u}^*\, d\bar{y}\right]_{\xi=\xi_b}$$

$$- \left[\bar{h}_2 \int_0^{\bar{y}_{s\ell}} \bar{\rho}^*\, \bar{u}^*\, d\bar{y}\right]_{\xi=\xi_a} + \int_{\xi_a}^{\xi_b}\int_0^{\bar{y}_{s\ell}} \bar{\rho}^* \frac{\partial \bar{v}^*}{\partial \eta} d\bar{y}\, \bar{h}_1\, d\xi \qquad (27)$$

The prime superscript refers to quantities associated with the boundary-layer flow, and the asterisk superscript refers to quantities in the inviscid flow field. The variable $\bar{y}$ is the dimensional distance normal to the body surface, and $\bar{y}_{s\ell}$ is the value of $\bar{y}$ on the inviscid separating line along which the boundary-layer outer-edge conditions are taken.

In treating the problem of streamline swallowing by the boundary layer in the windward symmetry plane of a blunt axisymmetric body, Eq. (27) is employed in an iteration scheme which results in determining $\bar{y}_{s\ell}$ (as a function of ξ) and the associated boundary-layer outer-edge conditions in a manner such that the final solution obtained for the boundary-layer equations satisfies Eq. (27). This iteration scheme is described in Section III.

The method which has just been described for determining $\bar{y}_{s\ell}$ and the outer-edge boundary conditions for the boundary-layer equations is applicable along the entire windward symmetry plane; however, since the present investigation is limited to cases for which the flow over the spherical nose cap is axisymmetric (with respect to the free-stream velocity vector passing through the stagnation point) up to the sphere-aft body

tangent point on the windward side, a simpler and more conventional global mass balance scheme, as used in Ref. 2, for example, has been used to treat the nose region streamline-swallowing problem. This method matches the mass flow in the boundary layer to the free-stream mass flow in order to determine the inclination of the bow shock wave where a given streamline entering the boundary layer crossed the bow shock wave. This information, together with the surface pressure along the body, is sufficient to permit the calculation of the outer-edge conditions when streamline swallowing is being considered in an axisymmetric flow situation. The details of this procedure are described in Ref. 2.

The inviscid flow field data used in this investigation were obtained from results of the three-dimensional inviscid flow field calculation method of Ref. 15. This method computes the flow field properties at points on lines normal to the body at consecutive locations along the body, in equally spaced planes around the body which contain the body axis.

In the neighborhood of the body surface the entropy, density, velocity, etc., but not the pressure, computed by methods for inviscid flow, change rapidly in the direction normal to the body surface. This is caused by the bow shock wave strength variation associated with the different streamlines in this region. This region of large gradients in the direction normal to the body surface is generally referred to as the inviscid "entropy layer" because of its relation to the entropy change across the bow shock wave. These gradients (or the associated bow shock wave strength variations) are, of course, the origin of the streamline-swallowing influences on boundary-layer data.

SECTION III
NUMERICAL SOLUTION METHOD

The numerical scheme used to solve the coupled nonlinear second-order partial differential Eqs. (7), (9), and (11), and the method used to determine the outer-edge boundary conditions through the treatment of the streamline-swallowing phenomenon are presented in this section. The body under consideration is a spherically blunted axisymmetric body with the flow in the windward plane of symmetry being treated. Basically, Eqs. (7), (9), and (11) are replaced by a set of consistent linearized algebraic equations. This set is of tridiagonal form and is solved by means of an especially efficient algorithm. The finite-difference scheme used is an implicit one, chosen because of the lack of problems with stability and mesh size, as opposed to explicit schemes.

The derivatives with respect to ξ are replaced by a finite-difference formulation which follows that introduced by Crank and Nicholson (Ref. 16). The set of finite-difference equations which is developed is uniformly valid to second-order in the mesh spacing of the finite-difference grid. In general, the a-terms given in Eqs. (8), (10), and (12) are assumed to be known. This results in the uncoupling and linearization of the set of equations which must be solved. This assumption is removed by recalculating the a-terms in an iteration on the solution to the set of finite-difference equations. In addition to

this iteration, there is a second iteration involved in determining the outer-edge boundary conditions through the mass-balance treatment of the streamline-swallowing phenomenon. Figure 5 shows these iteration procedures in a simplified flow chart of the digital computer program used to solve the finite-difference equations at a general point on the body. All computations made in this investigation were performed on a Control Data Corporation Model 1604B digital computer.

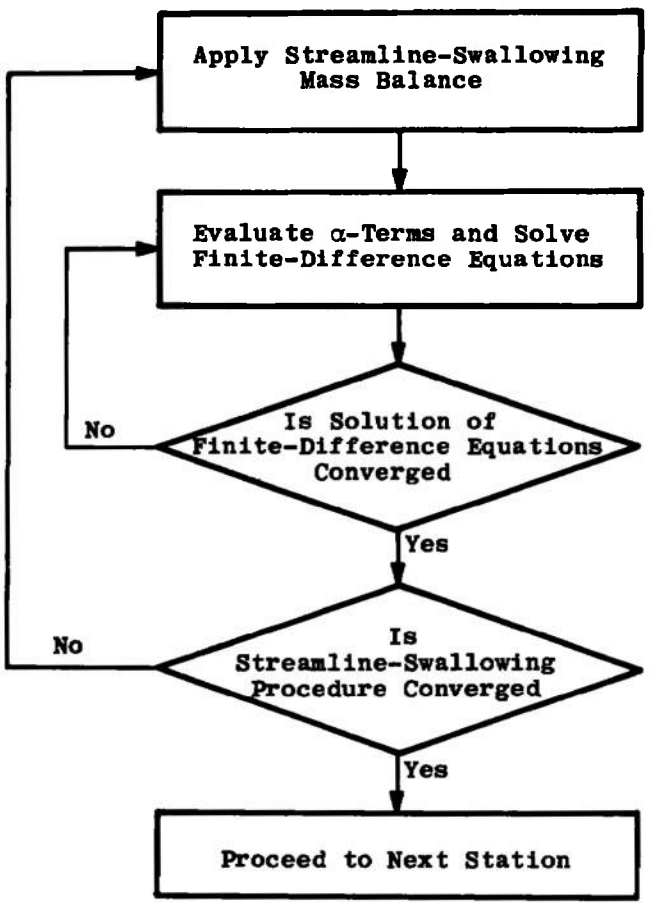

Fig. 5 Simplified Flow Diagram for Solution at a General Station

The explicit form of the coordinate system and the metric coefficients used may be described with reference to Fig. 6. The spherical nose cap is tangent to the axisymmetric aft body, with θ_c being the body slope with respect to the axis of symmetry at the tangency. The coordinate ζ is normal to the body surface and ξ is along the windward symmetry line of the body surface. Figure 6 actually represents two coordinate systems in that for the spherical nose cap η is the angular displacement from the windward symmetry plane about an axis containing the stagnation point and the center of the sphere, while for the aft body η is the angular displacement from the windward symmetry plane about the body axis.

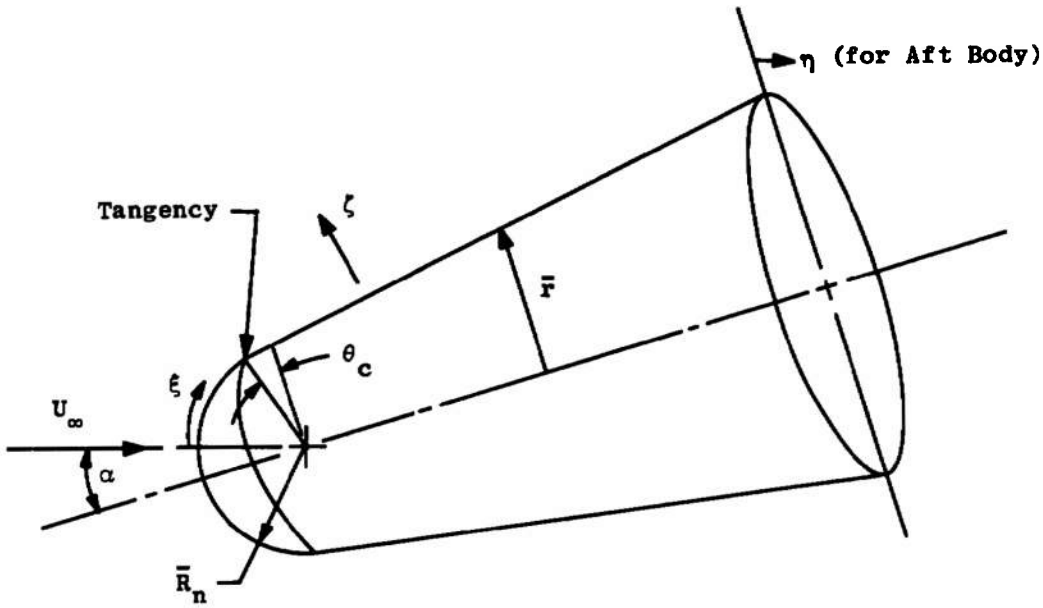

Fig. 6 Coordinate System

If the reference length $\bar{L}$ is defined to be the nose radius $\bar{R}_n$, then for the nose region the metric coefficients h_1 ahd h_2 are

$$h_1 = 1.0$$

$$h_2 = \sin \xi \tag{28}$$

The appearance of the group Z^2/h_2 in the AX coefficients makes the choice $Z^2 = \sin \xi$ attractive; however, since Φ is proportional to Z over $\bar{h}_3$, the selection of $Z^2 = \sin \xi$ would require $\bar{h}_3$ to be zero at ξ equal to zero in order to obtain a nonzero Φ. This situation makes the choice Z = 1.0 more reasonable and, in fact, the AX terms involving Z^2/h_2 lead to no difficulties even when $h_2 = 0$ at $\xi = 0$.

For ξ greater than $\pi/2 - \theta_c - \alpha$, i.e., past the tangent point, it is convenient to continue using $\bar{L} = \bar{R}_n$ and Z = 1.0. This leads to the following forms for h_1 and h_2 for the aft body

$$h_1 = 1.0$$

$$h_2 = \bar{r}/\bar{R}_n \equiv r \tag{29}$$

where $\bar{r}$ is the local radius of the body.

The use of two different coordinate systems causes no difficulty, since the overall problem is treated in three phases. First, the boundary-layer problem reduces to a two-point boundary-value problem (with independent variable ζ) at the stagnation point; second, the boundary-layer flow over the sphere is axisymmetric and the crossflow momentum equation need not be solved in this region; finally, the full three-dimensional boundary layer must be solved past the tangency point.

Since the governing equations are parabolic in the ξ direction, the entire solution can be obtained by a marching technique, with the results from each region providing the beginning data for the solution in the succeeding region. The following subsections describe the method of solution used for the governing equations (a) at $\xi = 0$, the stagnation point, (b) for ξ less than $\pi/2 - \theta_c - a$, on the sphere, and (c) for ξ greater than $\pi/2 - \theta_c - a$, on the aft body, and the final subsection of this section describes the application of the mass-balance scheme described in the previous section.

3.1 STAGNATION POINT SOLUTION

At the stagnation point ($\xi = 0$) and on the spherical nose region where the flow is axisymmetric, only the longitudinal momentum equation and the energy equation need to be solved, since the crossflow velocity is everywhere zero. Because of this, AX(9), AX(10), AX(11), and AX(12) are not needed since they appear only in the crossflow momentum equation. At the stagnation point the remaining AX terms have the following forms:

$$
\begin{aligned}
AX(1) &= 0 \\
AX(2) &= 0 \\
AX(3) &= \frac{\gamma}{\gamma-1}\, 2p\, \frac{\partial u_e}{\partial \xi} \\
AX(4) &= 0 \\
AX(5) &= \frac{\gamma}{\gamma-1}\, p\, \frac{\partial u_e}{\partial \xi} \\
AX(6) &= 0 \\
AX(7) &= 0 \\
AX(8) &= \frac{\partial^2 p}{\partial \xi^2} \Big/ \frac{\partial u_e}{\partial \xi} \\
AX(13) &= 0 \\
AX(14) &= 0
\end{aligned}
\tag{30}
$$

In obtaining these forms L'Hospital's rule has been utilized extensively, together with the fact that the derivatives with respect to η which appear are zero everywhere on the spherical nose. Although not rigorously correct, it has been assumed that $\partial u_e/\partial \xi$ at the stagnation point can be evaluated using Euler's equation

$$u_e \frac{\partial u_e}{\partial \xi} = - \frac{1}{\rho_e} \frac{\partial p}{\partial \xi}$$

to obtain $\partial u_e/\partial \xi$ as

$$\left(\frac{\partial u_e}{\partial \xi}\right)^2 = - \frac{1}{\rho_e} \frac{\partial^2 p}{\partial \xi^2}$$

at the stagnation point. This is equivalent to neglecting the effects of streamline swallowing on $\partial u_e/\partial \xi$ at the stagnation point, although certain concessions, mentioned later, are made to streamline-swallowing influences at $\xi = 0$. The values used for ρ_e and p at the stagnation point were those corresponding to stagnation conditions behind a normal shock in the freestream. The second derivative of p with respect to ξ was obtained by a least squares curve fit of the pressure data obtained from the method of Ref. 15. Specifically, the coefficient m in

$$\frac{p - p_\infty}{p_{\xi=0} - p_\infty} = \cos^m \xi$$

was determined, and the second derivative of this expression used for the required second derivative. (A value of m = 2 corresponds to the classical Newtonian approximation.)

Introducing the AX terms given in Eq. (30) into the boundary-layer equations as given in Eqs. (7), (8), (11), and (12) yields the following general form for the governing equations at $\xi = 0$, where X represents Φ or θ.

$$\frac{\partial^2 X}{\partial \zeta^2} + \alpha_{X1} \frac{\partial X}{\partial \zeta} + \alpha_{X3} = 0 \tag{31}$$

where

$$\alpha_{\Phi 1} = AX(5) \frac{\mu \zeta^2}{\Phi^2 T} + AX(8) \frac{\mu}{\Phi^2}$$

$$\alpha_{\Phi 3} = \frac{\mu}{\Phi T}\left\{AX(3)\zeta + AX(5)\left[\frac{\zeta^2}{T} \frac{\partial T}{\partial \xi} - 2\zeta - \frac{\zeta^2}{\mu} \frac{\partial \mu}{\partial \zeta}\right] - AX(8) \frac{T}{\mu} \frac{\partial \mu}{\partial \zeta}\right\}$$

$$\alpha_{\theta 1} = \frac{(1-Pr)}{\Phi} \frac{\partial \Phi}{\partial \zeta} + AX(5) \frac{\mu Pr}{\Phi^2 T} \zeta^2 + AX(8) \frac{\mu Pr}{\Phi}$$

$$- \frac{1}{Pr} \frac{\partial Pr}{\partial \zeta}$$

$$\alpha_{\theta 3} = 0 \tag{32}$$

The set of equations represented by Eq. (31) is a set of coupled, nonlinear, second-order ordinary differential equations. The independent variable is ζ, and the primary dependent variables are Φ and θ, with boundary conditions known at $\zeta = 0$ and $\zeta = 1.0$.

In order to cast Eq. (31) into an appropriate finite-difference form, a grid is established which divides the region from $\zeta = 0$ to $\zeta = 1$ into NZ - 1 equal increments with NZ grid points. At each interior point finite-difference forms for the first and second derivatives with respect to ζ are obtained from Taylor series truncation as

$$\left(\frac{\partial X}{\partial \zeta}\right)_n = \frac{X_{n+1} - X_{n-1}}{2\,\Delta\zeta} + O(\Delta\zeta^2)$$

$$\left(\frac{\partial^2 X}{\partial \zeta^2}\right)_n = \frac{X_{n+1} - 2X_n + X_{n-1}}{\Delta\zeta^2} + O(\Delta\zeta^2) \tag{33}$$

where $\Delta\zeta = 1/(NZ-1)$, and $O(\Delta\zeta^2)$ means that the lowest order terms which have been neglected in the Taylor series development are of the form $\Delta\zeta^2$ times some quantity which is independent of $\Delta\zeta$. The subscript n denotes the grid point under consideration, where n = 1 refers to $\zeta = 0$ and n = NZ refers to $\zeta = 1$.

The resulting finite-difference equivalent of Eq. (31) is

$$X_n = A_{X,n} X_{n+1} + B_{X,n} X_{n-1} + C_{X,n} \tag{34}$$

The explicit forms of A, B, and C are

$$A_{X,n} = \frac{2 + \alpha_{X1,n}\,\Delta\zeta}{4}$$

$$B_{X,n} = \frac{2 - \alpha_{X1,n}\,\Delta\zeta}{4}$$

$$C_{X,n} = \frac{\alpha_{X3,n}\,\Delta\zeta^2}{2} \tag{35}$$

In the evaluation of the finite-difference forms of the a-terms, all of the quantities involved are taken from an initial approximation or the previous iteration, and may, therefore, be considered known. The quantities involved in the derivatives in Eq. (31) are treated as unknowns and ultimately appear as the unknowns in Eq. (34).

An equation of the form of Eq. (34) is written for each value of n between 1 and NZ, assuming that Φ and θ are known at $\zeta = 0$ and $\zeta = 1$; however, for n = 2 the coefficients so determined for the Φ equation must be modified to take into account the surface boundary condition on Φ given by Eq. (25). For zero surface mass transfer, the boundary condition reduces to

$$\left(\frac{\partial \Phi}{\partial \zeta}\right)_{\zeta=0} = AX(8)\left(\frac{\mu}{\Phi}\right)_{\zeta=0} \tag{36}$$

Applying a finite-difference relation of $0(\Delta\zeta^2)$ accuracy to Eq. (36) yields

$$\Phi_1 = -\frac{2}{3}\,\Delta\zeta\,AX(8)\left(\frac{\mu}{\Phi}\right)_{\zeta=0} + \frac{4}{3}\,\Phi_2 - \frac{1}{3}\,\Phi_3 \tag{37}$$

where the subscripts represent the grid locations, with the subscript "1" being the node on the surface. From Eq. (34)

$$\Phi_2 = A^+_{\Phi,2}\,\Phi_3 + B^+_{\Phi,2}\,\Phi_1 + C^+_{\Phi,2} \tag{38}$$

where the plus superscripts refer to forms obtained assuming Φ_1 to be known. Eliminating Φ_1 from Eqs. (37) and (38) yields the coefficients which may be applied to take into account the surface derivative boundary condition on Φ,

$$A_{\phi,2} = \frac{A^+_{\phi,2} - \frac{1}{3}B^+_{\phi,2}}{1 - \frac{4}{3}B^+_{\phi,2}}$$

$$B_{\Phi,2} = 0$$

$$C_{\Phi,2} = \frac{-\frac{2}{3}\Delta\zeta\,AX(8)\left(\frac{\mu}{\Phi}\right)_{\zeta=0} B^+_{\Phi,2} + C^+_{\Phi,2}}{1 - \frac{4}{3}B^+_{\Phi,2}} \tag{39}$$

Equation (26) yields an outer-edge boundary condition on Φ of $\Phi = 0$ if streamline-swallowing influences are neglected; however, this is not the case when streamline swallowing is being considered. Since no reasonable way presents itself for the determination of Φ at $\zeta = 1$, $\xi = 0$ when streamline swallowing is being considered, the value of Φ used in these calculations was determined on the basis of experience. Although the value chosen had no significant effect on the stagnation point solution obtained, it was necessary to choose a value which was continuous with that determined for use in the solution at succeeding ξ locations on the spherical nose. The boundary conditions on θ are those given in Eq. (24). With the introduction of Eq. (39) and the boundary conditions just mentioned, the two sets of equations represented by Eq. (34) may be solved for the values of Φ and θ for $2 \leqslant n \leqslant NZ - 1$. The value of Φ_1 can be determined from Eq. (37) after the values of Φ_2 and Φ_3 are found. The value used for Φ_1 where it appears on the right hand side of Eq. (37) was that from the previous iteration.

The solution of the two sets of equations of the form of Eq. (34) was performed by the standard methods for linear tridiagonal algebraic systems. The particular form of Eq. (34) is that used by Patankar and Spalding, Ref. 10, and it has the advantage of requiring less computer storage than forms which involve four coefficient terms rather than three. Knowing the values of the dependent variables at n = 1 and n = NZ (corresponding to $\zeta = 0$ and $\zeta = 1$, respectively) except for Φ_1, which need not be known according to the treatment given previously, each of the sets of equations represented by Eq. (34) may be solved for X_2 through X_{NZ-1} by applying

$$X_n = P_n X_{n+1} + Q_n$$

where

$$P_n = \frac{A_{X,n}}{1 - B_{X,n} P_{n-1}}$$

$$Q_n = \frac{B_{X,n} Q_{n-1} + C_{X,n}}{1 - B_{X,n} P_{n-1}}$$

with

$$P_2 = A_{X,2}$$

$$Q_2 = B_{X,2} X_1 + C_2 \tag{40}$$

The set of P's and Q's can be determined consecutively from n = 2 through n = NZ-1, and the set of values of X_n may be determined beginning with n = NZ - 1 and proceeding to n = 2. The procedure indicated by Eq. (40) may be considered a special case of the Gaussian elimination procedure.

After solving the equations represented by Eq. (34), the a-terms are recomputed, using the results of the solution, and the equations are solved again. This procedure is repeated until the solution converges, i.e., until the difference between successive solutions is sufficiently small.

3.2 SOLUTION FOR THE SPHERICAL NOSE REGION

On the spherical nose cap where the flow is axisymmetric, it is necessary to solve only the longitudinal momentum equation and the energy equation. The stagnation point solution, obtained as described in the previous subsection, provides initial data for a "marching" scheme which solves the governing equations at successively greater values of ξ up to and including the sphere-aft body tangent point. If the outer-edge boundary conditions are taken to be the inviscid surface data, then solutions of the classical type are obtained.

On the windward symmetry line of the spherical nose cap the required AX coefficients have the following forms

$$
\begin{aligned}
AX(1) &= \frac{\gamma}{\gamma-1} u_e p \\
AX(2) &= 0 \\
AX(3) &= \frac{\gamma}{\gamma-1} \left(p \frac{\partial u_e}{\partial \xi} + u_e \frac{\partial p}{\partial \xi} + \frac{p u_e}{\tan \xi} \right) \\
AX(4) &= 0 \\
AX(5) &= \frac{\gamma}{\gamma-1} p \frac{\partial u_e}{\partial \xi} \\
AX(6) &= 0 \\
AX(7) &= 0 \\
AX(8) &= \frac{1}{u_e} \frac{\partial p}{\partial \xi} \\
AX(13) &= \frac{u_e^2}{He} \\
AX(14) &= 0
\end{aligned}
\tag{41}
$$

As at the stagnation point, AX(9), AX(10), AX(11), and AX(12) are not needed since they appear only in the crossflow momentum equation.

The introduction of Eq. (41) into Eqs. (7), (8), (11), and (12) yields the following general form for the governing equations on the spherical nose region

$$\frac{\partial^2 X}{\partial \zeta^2} + \alpha_{X1} \frac{\partial X}{\partial \zeta} + \alpha_{X3} + \alpha_{X4} \frac{\partial X}{\partial \xi} = 0 \tag{42}$$

where X represents Φ or θ.

The required α terms reduce to the following forms

$$\alpha_{\Phi 1} = AX(5) \frac{\mu \zeta^2}{\Phi^2 T} + AX(8) \frac{\mu}{\Phi^2}$$

$$\alpha_{\Phi 3} = \frac{\mu}{\Phi T} \left\{ AX(1) \left[\frac{\zeta}{\mu} \frac{\partial \mu}{\partial \xi} - \frac{\zeta}{T} \frac{\partial T}{\partial \xi} \right] + AX(3)\zeta \right.$$

$$\left. + AX(5) \left[-2\zeta - \frac{\zeta^2}{\mu} \frac{\partial \mu}{\partial \zeta} + \frac{\zeta^2}{T} \frac{\partial T}{\partial \zeta} \right] - AX(8) \frac{T}{\mu} \frac{\partial \mu}{\partial \zeta} \right\}$$

$$\alpha_{\Phi 4} = - AX(1) \frac{\mu \zeta}{\Phi^2 T}$$

$$\alpha_{\theta 1} = \frac{(1-Pr)}{\Phi} \frac{\partial \Phi}{\partial \zeta} - \frac{1}{Pr} \frac{\partial Pr}{\partial \zeta} + \alpha_{\Phi 1} Pr$$

$$\alpha_{\theta 3} = - AX(13) (1-Pr) \left(1 + \frac{\zeta}{\Phi} \frac{\partial \Phi}{\partial \zeta} \right) + AX(13) \frac{\zeta}{Pr} \frac{\partial Pr}{\partial \zeta}$$

$$\alpha_{\theta 4} = \alpha_{\Phi 4} Pr \tag{43}$$

In order to numerically treat Eq. (42), a finite-difference grid is established over the region $0 < \xi \leqslant \pi/2 - \alpha - \theta_c$, $\eta = 0$, $0 \leqslant \zeta \leqslant 1$. The grid has uniform step sizes in both the ξ and ζ directions, although a constant step size in only ζ is required for the finite-difference scheme which is used. The scheme which is used employs the known data at a given value of ξ in determining the solution at the succeeding ξ-grid location. If the solution is known at the typical ξ location indicated by the subscript i=1 and is to be found at the ξ location indicated by i=2, where $X_{i,j}$ indicates the value of the

variable X at the ξ location i and the ζ-grid location j, then the finite-difference expressions needed to cast Eq. (42) into finite-difference form at the point (0,n) indicated in Fig. 7 are the following

$$X_{0,n} = \frac{X_{1,n} + X_{2,n}}{2} + O(\Delta^2)$$

$$\left(\frac{\partial X}{\partial \xi}\right)_{0,n} = \frac{X_{2,n} - X_{1,n}}{\Delta\xi} + O(\Delta^2)$$

$$\left(\frac{\partial X}{\partial \zeta}\right)_{0,n} = \frac{X_{1,n+1} + X_{2,n+1} - X_{1,n-1} - X_{2,n-1}}{4\Delta\zeta} + O(\Delta^2)$$

$$\left(\frac{\partial^2 X}{\partial \zeta^2}\right)_{0,n} = \frac{X_{1,n+1} + X_{2,n+1} - 2X_{1,n} - 2X_{2,n} + X_{1,n-1} + X_{2,n-1}}{2\Delta\zeta^2} + O(\Delta^2) \tag{44}$$

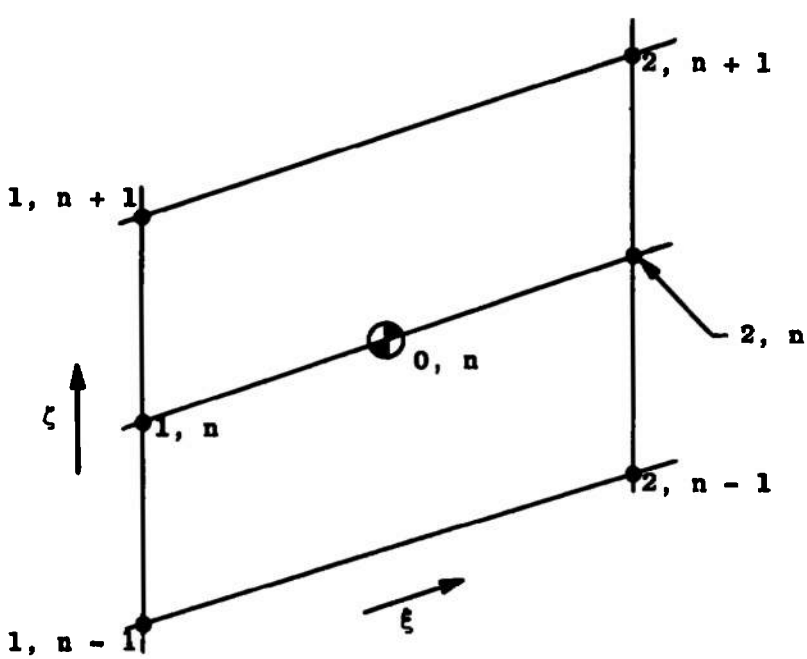

Fig. 7 Typical Section of Finite-Difference Grid for $0 < \xi \leq \pi/2 - \alpha - \theta_c$

where $\Delta\zeta$ is described previously, $\Delta\xi = (\pi/2\text{-}a\text{-}\theta_c)/(\text{NSPH-1})$, and NSPH-1 is the number of ξ increments between the stagnation point and the tangency point. In Eq. (44), $0(\Delta^2)$ implies that the lowest order terms which have been neglected are of the form of a second-order term in $\Delta\xi$ or $\Delta\zeta$ times some quantity which is independent of the mesh spacing. The forms given in Eq. (44) are consistent with those of Crank and Nicholson (Ref. 16), and their introduction into Eq. (42) yields the following general form for the corresponding finite-difference equation

$$X_{2,n} = A_{X,n}\, X_{2,n+1} + B_{X,n}\, X_{2,n-1} + C_{X,n} \tag{45}$$

where A, B, and C are evaluated at (0,n). The explicit forms of A, B, and C are

$$A_{X,n} = \frac{\dfrac{1}{2\Delta\zeta^2} + \dfrac{\alpha_{X1}}{4\Delta\zeta}}{\dfrac{1}{\Delta\zeta^2} - \dfrac{\alpha_{X4}}{\Delta\xi}}$$

$$B_{X,n} = \frac{\dfrac{1}{2\Delta\zeta^2} - \dfrac{\alpha_{X1}}{4\Delta\zeta}}{\dfrac{1}{\Delta\zeta^2} - \dfrac{\alpha_{X4}}{\Delta\xi}}$$

$$C_{X,n} = \frac{1}{\dfrac{1}{\Delta\zeta^2} - \dfrac{\alpha_{X4}}{\Delta\xi}} \left\{ X_{1,n}\left(-\frac{1}{\Delta\zeta^2} - \frac{\alpha_{X4}}{\Delta\xi}\right) + X_{1,n+1}\left(\frac{1}{2\Delta\zeta^2} + \frac{\alpha_{X1}}{4\Delta\zeta}\right) + X_{1,n-1}\left(\frac{1}{2\Delta\zeta^2} - \frac{\alpha_{X1}}{4\Delta\zeta}\right) + \alpha_{X3} \right\} \tag{46}$$

For X equal to each of Φ and θ an equation of the form of Eq. (45) can be written for $1 < n < NZ$, where the surface boundary condition on Φ is treated as discussed previously. The outer boundary condition on Φ is discussed in the last part of this section. The boundary conditions on θ are as given in Eq. (24). The method used for the determination of the outer-edge data required for the AX coefficients is discussed in the last subsection of this section. These coefficients are evaluated at $\xi = (\xi_1 + \xi_2)/2$. The a terms appearing in Eq. (46) are evaluated at the point (0,n) using the forms given in Eq. (44).

Generally, all of the data required in the a terms are treated as known, using initial approximations or results from the previous iteration. Thus, the two sets of equations represented by Eq. (45) can be solved by the application of Eq. (40). The iteration scheme previously described is used to eliminate the assumption made concerning the a terms. Using the solution obtained at the stagnation point as the initial known set of data, the solution method may be applied at consecutively increasing values of ξ, with each solution obtained providing the known solution for the next step. The solution obtained at the sphere-aft body tangency is used to provide the initial data for continuing the solution on the aft body, as described in the next subsection.

3.3 SOLUTION FOR THE AFT BODY

On the axisymmetric aft body the coordinate system changes so that η is measured about the body axis of symmetry. This was discussed previously in connection with Fig. 6. Also, on the aft body the crossflow momentum equation must be considered since the flow is not axisymmetric past the tangency location.

The AX coefficients for the windward symmetry plane of the aft body take the following forms

$$AX(1) = \frac{\gamma}{\gamma-1} u_e p$$

$$AX(2) = 0$$

$$AX(3) = \frac{\gamma}{\gamma-1} \left(p \frac{\partial u_e}{\partial \xi} + u_e \frac{\partial p}{\partial \xi} + \frac{p u_e}{r} \frac{\partial r}{\partial \xi} \right)$$

$$AX(4) = \frac{\gamma}{\gamma-1} \frac{p}{r} \frac{\partial v_e}{\partial \eta}$$

$$AX(5) = \frac{\gamma}{\gamma-1} p \frac{\partial u_e}{\partial \xi}$$

$$AX(6) = 0$$

$$AX(7) = 0$$

$$AX(8) = \frac{1}{u_e} \frac{\partial p}{\partial \xi}$$

$$AX(9) = 0$$

$$AX(10) = \frac{\gamma}{\gamma-1} u_e p \left(\frac{\partial}{\partial \xi} \left(\frac{\partial v_e}{\partial \eta} \right) \Big/ \frac{\partial v_e}{\partial \eta} + \frac{1}{r} \frac{\partial r}{\partial \xi} \right)$$

$$AX(11) = \frac{\gamma}{\gamma-1} \frac{p}{r} \frac{\partial v_e}{\partial \eta}$$

$$AX(12) = \frac{1}{r} \frac{\partial^2 p}{\partial \eta^2} \Big/ \frac{\partial v_e}{\partial \eta}$$

$$AX(13) = u_e^2/He$$

$$AX(14) = 0 \tag{47}$$

Thus, for $\xi > \pi/2 - a - \theta_c$, $\eta = 0$, the governing equations have the general form

$$\frac{\partial^2 X}{\partial \zeta^2} + \alpha_{X1} \frac{\partial X}{\partial \zeta} + \alpha_{X2} X + \alpha_{X3} + \alpha_{X4} \frac{\partial X}{\partial \xi} = 0 \tag{48}$$

where X represents Φ, G, or θ. The a terms take on the following forms

$$\alpha_{\Phi 1} = \frac{\mu}{\Phi^2} \left(AX(5) \frac{\zeta^2}{T} + AX(8) \right)$$

$$\alpha_{\Phi 2} = 0$$

$$\alpha_{\Phi 3} = \frac{\mu}{\Phi T} \left\{ AX(1) \left(\frac{\zeta}{\mu} \frac{\partial \mu}{\partial \xi} - \frac{\zeta}{T} \frac{\partial T}{\partial \xi} \right) + AX(3)\zeta \right.$$

$$\left. + AX(4)G + AX(5) \left(-2\zeta - \frac{\zeta^2}{\mu} \frac{\partial \mu}{\partial \zeta} + \frac{\zeta^2}{T} \frac{\partial T}{\partial \zeta} \right) - AX(8) \frac{T}{\mu} \frac{\partial \mu}{\partial \zeta} \right\}$$

$$\alpha_{\Phi 4} = - AX(1) \frac{\mu \zeta}{\Phi^2 T}$$

$$\alpha_{G1} = \alpha_{\Phi 1}$$

$$\alpha_{G2} = - AX(10) \frac{\mu \zeta}{\Phi^2 T} - AX(11) \frac{\mu G}{\Phi^2 T}$$

$$\alpha_{G3} = - AX(12) \frac{\mu}{\Phi^2}$$

$$\alpha_{G4} = \alpha_{\phi 4}$$

$$\alpha_{\theta 1} = \frac{(1-Pr)}{\Phi}\frac{\partial\Phi}{\partial\zeta} - \frac{1}{Pr}\frac{\partial Pr}{\partial\zeta} + \alpha_{\phi 1}\, Pr$$

$$\alpha_{\theta 2} = 0$$

$$\alpha_{\theta 3} = -\, AX(13)(1-Pr)\left(1 + \frac{\zeta}{\Phi}\frac{\partial\Phi}{\partial\zeta}\right) + AX(13)\,\frac{\zeta}{Pr}\frac{\partial Pr}{\partial\zeta}$$

$$\alpha_{\theta 4} = \alpha_{\phi 4}\, Pr \tag{49}$$

The finite-difference treatment of Eq. (48) is essentially the same as that used for Eq. (42) on the spherical nose. The same finite-difference grid indicated in Fig. 7 can be used, and the basic finite-difference relations given in Eq. (44) are applicable. Application of these finite-difference relations to Eq. (48) yields the general form for the corresponding finite-difference equation as

$$X_{2,n} = A_{X,n}\, X_{2,n+1} + B_{X,n}\, X_{2,n-1} + C_{X,n} \tag{50}$$

where

$$A_{X,n} = \frac{1}{D_{X,n}}\left(\frac{1}{2\Delta\zeta^2} + \frac{\alpha_{X1}}{4\Delta\zeta}\right)$$

$$B_{X,n} = \frac{1}{D_{X,n}}\left(\frac{1}{2\Delta\zeta^2} - \frac{\alpha_{X1}}{4\Delta\zeta}\right)$$

$$C_{X,n} = A_{X,n}\, X_{1,n+1} + B_{X,n}\, X_{1,n-1}$$

$$+ \frac{1}{D_{X,n}}\left[X_{1,n}\left(\frac{\alpha_{X2}}{2} - \frac{\alpha_{X4}}{\Delta\xi} - \frac{1}{\Delta\zeta^2}\right) + \alpha_{X3}\right]$$

where

$$D_{X,n} = \frac{1}{\Delta\zeta^2} - \frac{\alpha_{X2}}{2} - \frac{\alpha_{X4}}{\Delta\xi} \tag{51}$$

The equations represented by Eq. (50) are solved for $X_{2,n}$ ($1 < n < NZ$) by the application of Eq. (40). The a terms in Eq. (51) are evaluated at the point (0,n) indicated in Fig. 7 through the use of Eq. (44). The a terms are treated through the iteration scheme described previously.

The boundary conditions on G and θ are those given in Eq. (24), and the surface boundary condition on Φ is treated as discussed in connection with Eq. (36).

The method used to determine outer-edge value of Φ and the values of u_e, $\partial v_e/\partial\eta$, etc., is discussed in the following section. Basically, the location of the inviscid separating line is initially approximated in some manner, and the necessary outer-edge conditions determined. The boundary-layer equations are then solved, and that solution used to determine again the location of the inviscid separating line and the concomitant outer-edge conditions. This procedure is repeated until a converged value is obtained for the location of the inviscid separating surface.

3.4 NUMERICAL TREATMENT OF STREAMLINE SWALLOWING

In Subsection 2.4 a mass balance scheme is presented which allows the boundary-layer outer-edge conditions to be determined in a manner which considers the entrainment of the inviscid flow by the boundary layer. The crux of the scheme is in the determination of the height above the body surface of the line in the inviscid flow field which separates that part of the inviscid flow which is entrained by the boundary layer from that which is not entrained by the boundary layer. An approach is described which is applicable along the entire windward symmetry plane; however, a simpler method is discussed for use over the spherical nose region where the flow is axisymmetric.

The global mass-balance method used to treat the streamline-swallowing phenomenon in the axisymmetric flow region was described generally in Subsection 2.4, and has been described in detail in many other reports (for example, Refs. 1, 2, and 3). In the present formulation, however, there is one consideration not usually treated elsewhere. This is, that in order to evaluate the outer-edge boundary condition to be applied to Φ, as given by Eq. (26), a value of du/dy is required. The value used is essentially the value of du/dy in the inviscid flow field on the inviscid separating line. In the axisymmetric flow region this has been done by considering the numerically evaluated velocity gradient between two closely spaced streamlines, with one being that crossing the inviscid separating surface at the given value of ξ and the other slightly displaced from the first.

The specific inviscid flow field data used in determining the outer-edge conditions over the aft body (obtained using the method of Ref. 15) are: (a) u, ρ, and $\partial v/\partial\eta$ as functions of $\bar{y}/\bar{R}_n$ (at a series of values of $\bar{y}/\bar{R}_n$, beginning with the body and ending with the shock wave) at a series of discrete consecutive values of ξ, beginning at the tangency point, and (b) p and $\partial^2 p/\partial\eta^2$ as functions of ξ only, at the same ξ locations as in (a). The method of solution for axisymmetric flow is continued up to and including the tangency location; beyond this location the three-dimensional nature of the flow must

be considered. The value of $\bar{y}_{s\ell}$ at the tangency location can be determined from knowing the mass flow in the boundary layer at that point from the axisymmetric region solution and finding the value of $\bar{y}_{s\ell}$ which matches the inviscid mass flow up to that height to the boundary mass flow. This quantity is needed in order to proceed down the body with the streamline-swallowing calculations.

In applying Eq. (27) to determine the outer-edge conditions at $\xi = \xi_b$, where $\bar{y}_{s\ell}$ and the boundary-layer solution at $\xi = \xi_a$ have already been obtained, the first step is to assume some approximate value of $\bar{y}_{s\ell}$ at $\xi = \xi_b$ (see Fig. 4 for ξ_a and ξ_b). This value allows the necessary outer-edge conditions to be determined from the inviscid flow field data, and the boundary-layer equations can then be solved. Having a solution to the boundary-layer equations at $\xi = \xi_b$, Eq. (27) can be applied to determine a new value of $\bar{y}_{s\ell}$ at $\xi = \xi_b$. This is used to obtain new outer-edge conditions, etc., and the entire procedure is repeated until $\bar{y}_{s\ell}$ at $\xi = \xi_b$ converges to the desired degree.

Equation (27) is treated numerically by using a straightforward trapezoidal rule integration for the single integrals, and the double integrals are treated similarly as

$$\int_{\xi_a}^{\xi_b} \int_0^{\tilde{\lambda}} f(\lambda,\xi)d\lambda \quad g(\xi)d\xi$$

$$= \frac{ja + jb}{2} \int_{\xi_a}^{\xi_b} g(\xi)\, d\xi \tag{52}$$

where

$$ja = \left[\int_0^{\tilde{\lambda}} f(\lambda,\xi)\, d\lambda \right]_{\xi = \xi_a}$$

$$jb = \left[\int_0^{\tilde{\lambda}} f(\lambda,\xi)\, d\lambda \right]_{\xi = \xi_b} \tag{53}$$

Since $g(\xi)$ in the integral on the right-hand side of Eq. (52) is just $\bar{h}_1$, this integral can be evaluated exactly; the integrals in Eq. (53) are treated by trapezoidal rule integration. After being operated on in the manner just discussed, Eq. (27) has in it two integrals of the form

$$\left[\int_0^{\bar{y}_{s\ell}} \ldots\ldots d\bar{y} \right]_{\xi=\xi_b} \tag{54}$$

If a solution to the boundary-layer equations is available at ξ_b, then all of the terms in Eq. (27) can be evaluated except those of the form of Eq. (54), where $\bar{y}_{s\ell}$ at ξ_b is not known. These integrals can be evaluated as a function of $\bar{y}$ at ξ_b, and that value of $\bar{y}$ which satisfies Eq. (27) is the value of $\bar{y}_{s\ell}$ at ξ_b which can be used to continue the streamline-swallowing iteration cycle.

In developing the nondimensional forms of the governing boundary-layer equations, the Reynolds number Re was eliminated as an explicit parameter, and the resulting partial differential equations were independent of the value of Re. If the boundary conditions and the auxiliary relations (equation of state, viscosity law, etc.) are also independent of Re, then the resulting solutions of the boundary-layer equations are independent of Re. This situation occurs for the case of laminar boundary-layer flow when the normal shock or inviscid body surface conditions are used as the outer-boundary conditions (this is the classical, or at least more conventional, method of treating the outer-boundary conditions). For turbulent flow, the transport laws used herein are not independent of Re, and the resulting solutions to the boundary-layer equations are, independent of streamline-swallowing considerations, functions of Re. When streamline swallowing is considered, the outer-edge conditions and the resulting solutions to the boundary-layer equations are dependent on the value of Re, even for laminar flow.

SECTION IV
RESULTS OF CALCULATIONS

In this section are presented the results of numerical experiments concerning the behavior of the solution method described in the previous section and comparisons of results from the present method with experimental data and the results of other methods of computation.

4.1 NUMERICAL EXPERIMENTS

A series of calculations was performed to investigate grid spacing, convergence criteria, and other factors involved in applying the finite-difference solution technique described

in Section III. The results of the calculations made in this investigation were augmented by the results of similar considerations described in Ref. 4.

It was determined that a practical value for the number of ζ grid lines was 51, yielding a value of $\Delta\zeta = 0.02$. Typically, 50 to 100 constant $\Delta\xi$ steps were used between the stagnation point and the tangency location. Beyond the tangency location, the ξ step was gradually increased (with ξ) to some value and then held constant so that at a value of $\xi = 20$; for example, a $\Delta\xi$ of 0.5 was reached, and $\Delta\xi$ was held constant beyond that ξ location.

The convergence of the iteration resulting from the linearization involving the a terms was determined by testing the change in the solution between successive iterations. The iteration was deemed sufficiently converged when the surface value of Φ varied less than 0.01 percent between successive iterations.

The convergence of the iteration used for the determination of the height of the inviscid separating surface above the body surface was determined through a comparison of the values of the height of the inviscid separating surface obtained from successive iterations. This iteration was deemed to be sufficiently converged when successive values differed by no more than 0.5 percent.

Following experience obtained in the investigation reported in Ref. 4, a straightforward "bootstrap" iteration scheme was not used in solving the boundary-layer equations. Instead, at each stage in the iteration procedure, the solution obtained was weighted with the results from the previous iteration before proceeding with the iteration. This treatment served to stabilize the iteration procedure, especially at the stagnation point.

4.2 COMPARISONS WITH EXPERIMENT AND OTHER CALCULATIONS

A preliminary test of the present method was to compare results with calculations made using the first-order Levy-Lees variables method presented in Ref. 17 for the treatment of laminar boundary-layer flow. The particular case treated was that of a 9-deg sphere-cone at zero incidence in a Mach 10.9 flow. The value of θ at the body surface was 0.25, and a value of $Re = 1.81 \times 10^6$ was used, although, since these test calculations omitted any streamline-swallowing influences, the results presented in similarity form in Figs. 8 and 9 are independent of the value of Re.

Figure 8 shows comparisons of the heat-transfer and skin friction distributions obtained by the present method with results obtained by the method of Ref. 17. The results from the two methods agree quite well over the entire length of body considered. Figure 9 shows comparisons of the velocity and total enthalpy profiles computed by the two methods at a value of $\xi = 2.5$. This figure shows excellent agreement between the results of the two methods. (In these and succeeding figures, ξ is the surface distance divided by the nose radius.)

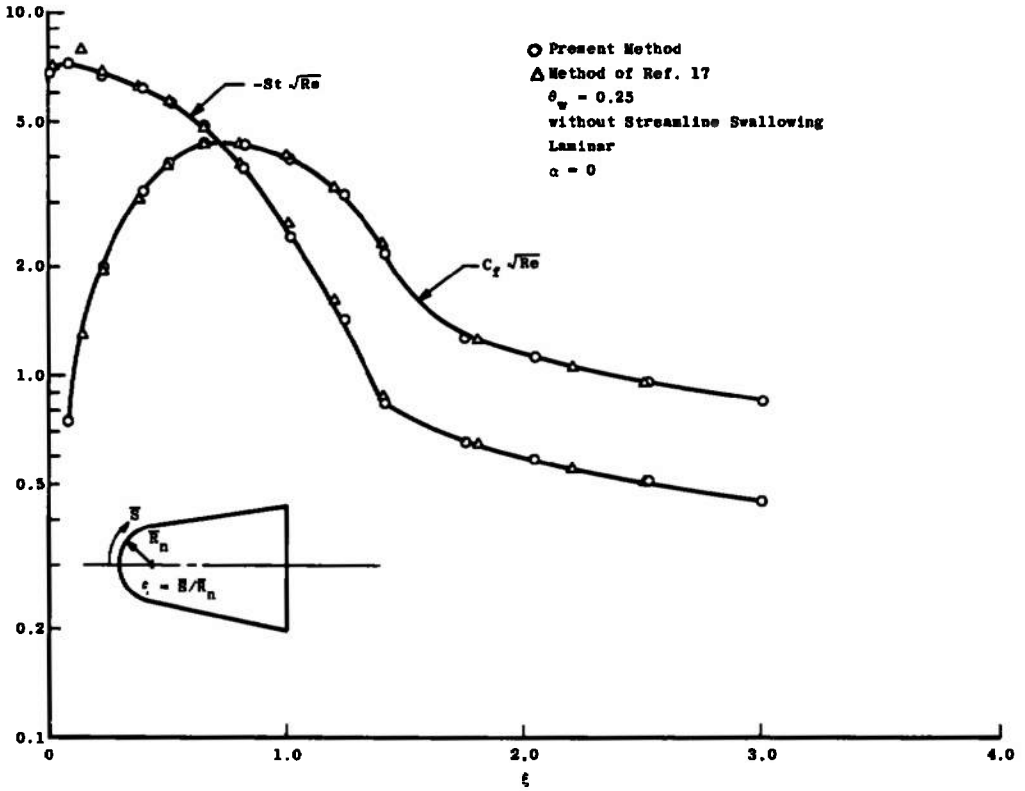

Fig. 8 Heat-Transer and Skin Friction Distributions on a 9-deg Sphere-Cone at Mach 10.9

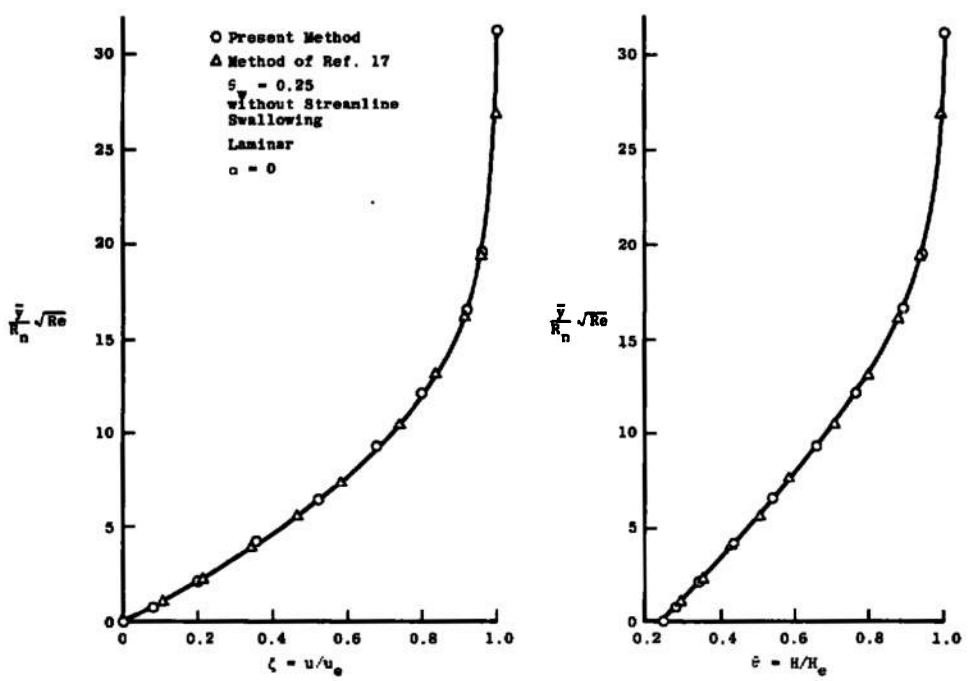

Fig. 9 Velocity and Total Enthalpy Profiles at ξ = 2.5 on a 9-deg Sphere-Cone at Mach 10.9

Figures 10 and 11 show comparisons of Stanton number distributions computed by the present method with experimental data reported in Ref. 18 for laminar boundary-layer flow over a 15-deg sphere-cone in a Mach 10.6 freestream. The value of θ_w is 0.27 and the angle of attack is 10 deg for both cases.

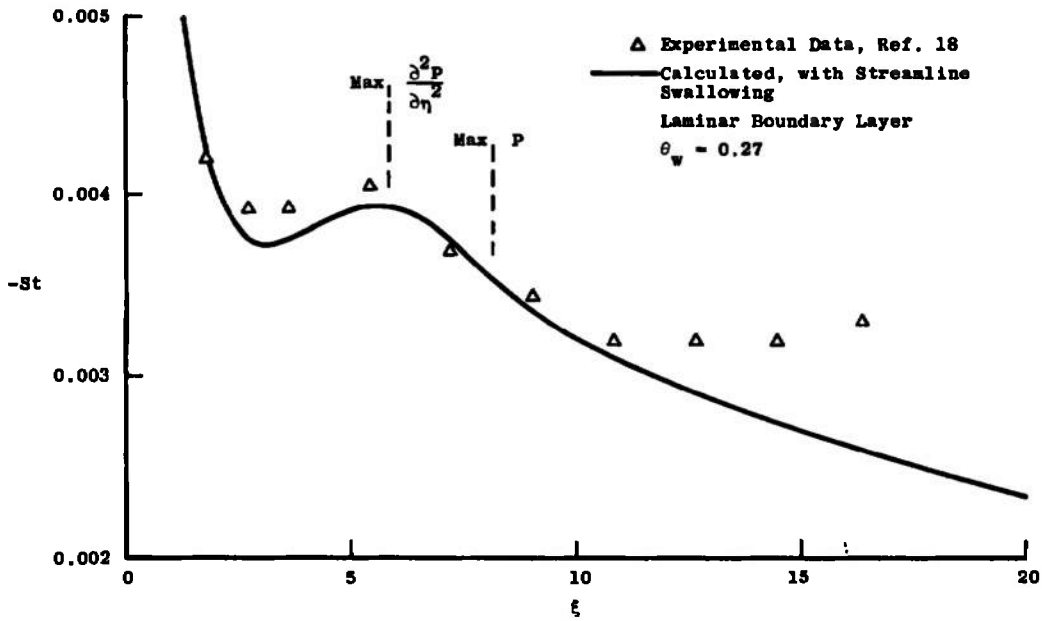

Fig. 10 Heat-Transfer Distribution on a 15-deg Sphere-Cone in a Mach 10.6 Flow at α = 10 deg and Re = 1.1 x 10^5

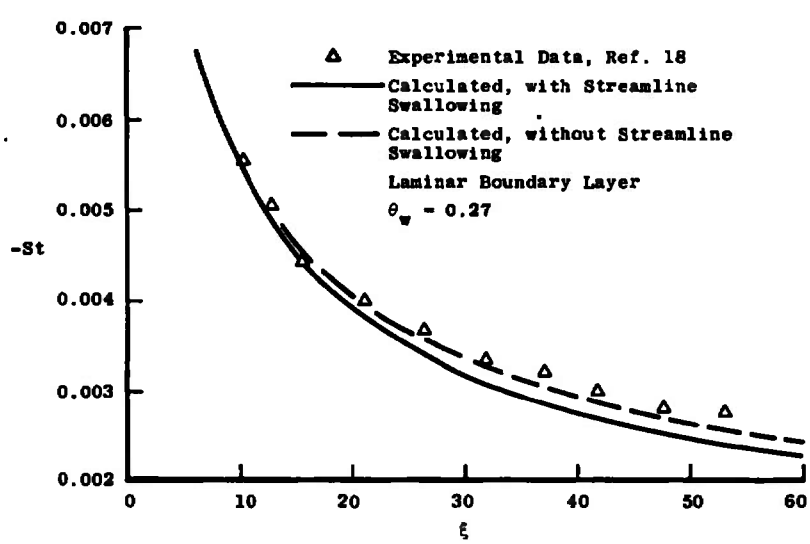

Fig. 11 Heat-Transfer Distribution on a 15-deg Sphere-Cone at α = 10 deg in a Mach 10.6 Flow with Re = 3.75 x 10^4

Figure 10 shows results for a value of Re = 1.1 x 10^5. The calculation results shown in Fig. 10 are based on including streamline-swallowing influences in the calculations. There is reasonably good agreement between the computed data and the experimental data up to a value of ξ of about 10. Beyond ξ = 10, the experimental data appear to indicate the onset of boundary-layer transition to turbulent flow. The relative maximum in the data at a value of ξ of approximately 5.5 appears in both the computed results and in the experimental data and can be related to the maximum (with respect to ξ) of $\partial^2 p/\partial\eta^2$ which occurs there. It is interesting to note that, although the boundary-layer flow and the heat-transfer rate must depend on the value of p, the maximum value of p in the recompression region occurs considerably past the maximum heating location.

Figure 11 shows a comparison of computed Stanton number distributions with experimental data for a value of Re = 3.75 x 10^4. These results show a reasonable agreement between the experimental data and the results of calculations neglecting streamline swallowing, with the results of calculations including streamline swallowing falling some 8 percent below the experimental data and the other computed results near the end of the body considered. No determination has been made concerning the reason for this discrepancy.

Figure 12 shows comparisons of computed Stanton number distributions with experimental data for the case of a 7.2-deg sphere-cone at α = 4 deg in a Mach 8 flow.

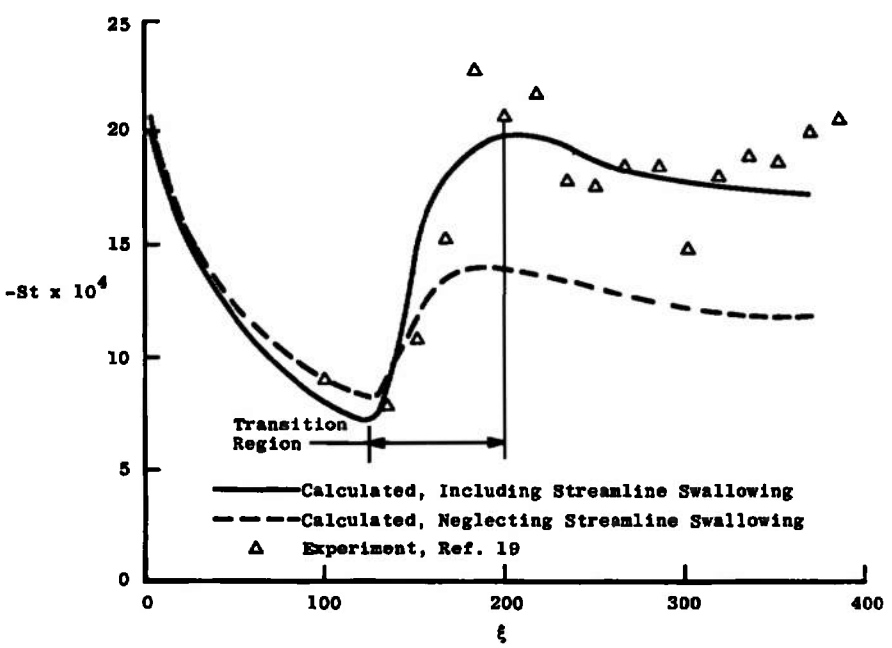

Fig. 12 Heat-Transfer Distribution on a 7.2-deg Sphere-Cone in a Mach 8 Flow at α = 4 deg and Re = 34467

The flow undergoes transition from laminar to turbulent flow between $\xi = 125$ and $\xi = 200$. The value of Re for this case is 34467, and $\theta_w = 0.395$. For those regions with transitional and turbulent boundary-layer flow, there is reasonably good agreement between the experimental data and the Stanton number distribution calculated when streamline-swallowing influences were considered. In the turbulent flow region, the results computed neglecting streamline swallowing are approximately 30 percent below the experimental data.

The data shown in Fig. 12 for the laminar flow region are similar to those in Fig. 11 in that the Stanton number computed, including streamline swallowing, lies below that computed neglecting streamline swallowing. This is in contrast to the typical result obtained at $\alpha = 0$, where the results computed including streamline-swallowing influences approach sharp cone data as ξ increases, and lie above the results obtained neglecting streamline swallowing. One reason for the difference between the results obtained in this investigation for $\alpha \neq 0$ and the typical $\alpha = 0$ results is that $\partial v/\partial \eta$ in the inviscid entropy layer is maximum at the body surface, and decreases to the sharp cone level at the outer edge of the entropy layer (over the aft part of the body, for, say, $\xi > 10$). Thus, this crossflow influence, which is subject to change due to streamline swallowing, actually decreases with the consideration of streamline swallowing, and as $\partial v_e/\partial \eta$ decreases so does the surface heat flux. It is also noteworthy that even though p reaches a value near the sharp cone value at $\xi = 30$ and varies little beyond there, $\partial^2 p/\partial \eta^2$ for this sphere-cone case decreases to about one-third of the sharp cone value at $\xi = 200$ and increases to only about one-half of the sharp cone value at $\xi = 375$. These comments depend, of course, on the validity of the inviscid flow field computations, and for this case where the inviscid entropy layer is described by only three or four points (in the direction normal to the body surface) over the aft part of the body, the validity of the inviscid computations may be suspect.

Figures 13, 14, and 15 show comparisons of computed and measured Stanton number data on 11- and 14-deg sphere-cones in a Mach 8 freestream. Each figure shows the variation of St with α at a given ξ location. (The ξ locations given in the captions of Figs. 13, 14, and 15 are those in effect at $\alpha = 0$. Since ξ is measured from the stagnation point of the flow, the ξ value for a fixed point decreases as α increases. The change is only -0.35 for $\alpha = 20$ deg). These experimental data were taken in the AEDC/VKF Hypersonic Wind Tunnel (B). The turbulent boundary-layer results were obtained with the boundary layer tripped at ξ locations of approximately 4, 2, and 3, for the data of Figs. 13, 14, and 15, respectively. The calculated data for $\alpha = 0$ were obtained using the method of Ref. 3; the calculated data for $\alpha > 0$ were obtained using the method described in this report (calculations were performed for $\alpha = 5$, 10, 15, and 20 deg). All of the calculations included the influences of streamline swallowing on the outer-edge boundary conditions, although on these relatively short bodies these effects were not strong. The agreement between the calculations and the experimental data is quite good in each of Figs. 13, 14, and 15 for both the laminar and turbulent flow cases, and for angles of attack up to almost twice the cone half-angle, a condition for which crossflow influences should be strong.

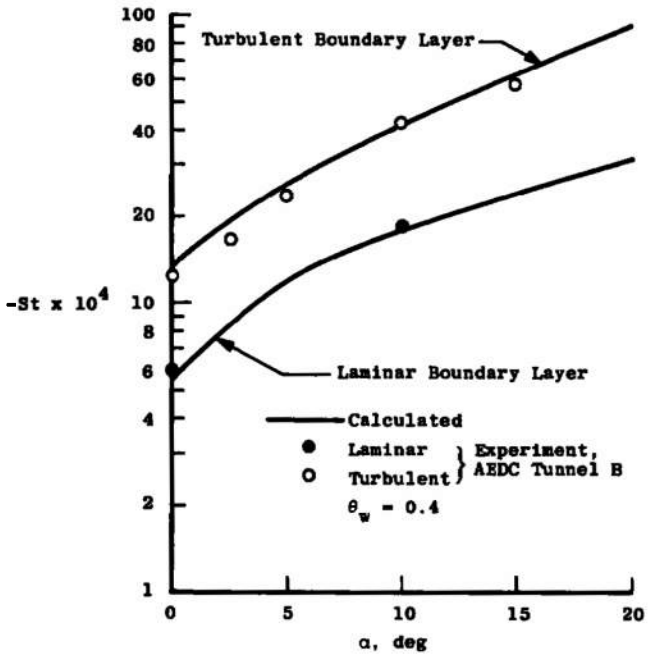

Fig. 13 Comparisons of Computed and Measured Stanton Numbers at ξ = 11.9 on an 11-deg Sphere-Cone at Mach 8 as a Function of α at Re = 1.75 x 10^5

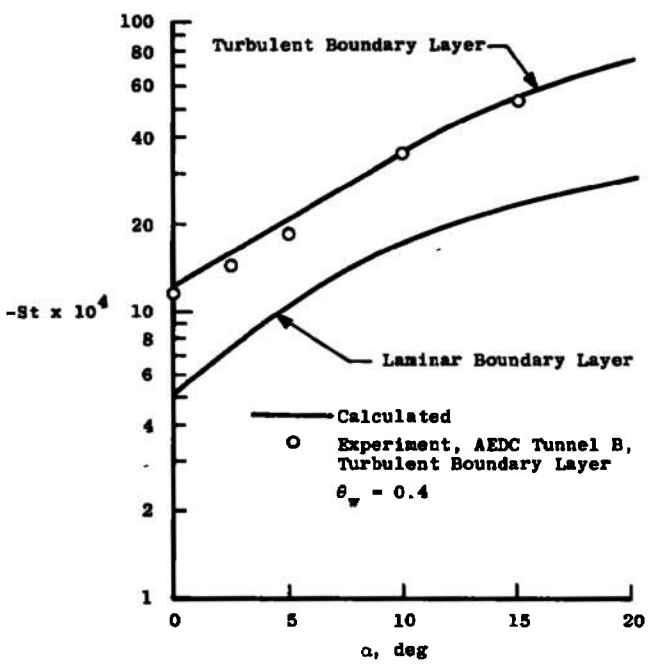

Fig. 14 Comparisons of Computed and Measured Stanton Numbers at ξ = 7.5 on an 11-deg Sphere-Cone at Mach 8 as a Function of α at Re = 2.33 x 10^5

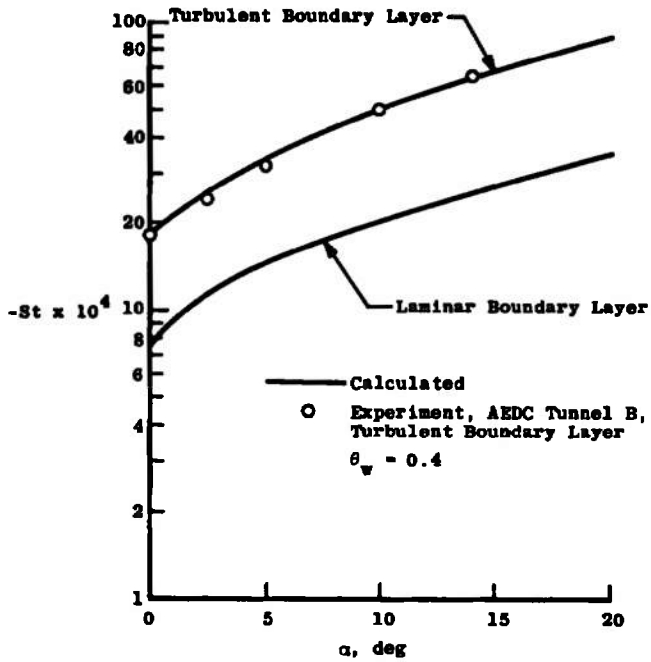

Fig. 15 Comparisons of Computed and Measured Stanton Numbers at ξ = 9.3 on a 14-deg Sphere-Cone at Mach 8 as a Function of α at Re = 1.75 x 10^5

SECTION V
RESULTS AND DISCUSSION

The three-dimensional compressible boundary-layer equations have been developed in a Crocco-variables form for treating the flow in the windward symmetry plane of a spherically blunted aximmetric body at angle of attack under hypersonic conditions. Through the use of an eddy transport coefficient hypothesis and a streamwise intermittency factor, both transitional and fully turbulent boundary layers may be treated, in addition to laminar boundary-layer flow. A method was also presented for determining the outer-edge boundary conditions to be applied to the boundary-layer equations, through a mass flow balance treatment of the boundary-layer entrainment of the inviscid flow over the body. A finite-difference technique was presented for solving the set of governing partial differential equations and for treating the streamline-swallowing phenomenon.

The treatment of the problem was validated by the good agreement obtained between results from the present method and both experimental data and results from other methods of calculation (at zero angle of attack). Comparisons with experimental data were made for both laminar and turbulent boundary-layer flow, and included cases where streamline-swallowing effects were large and cases where crossflow influences should be strong.

Recommended extensions to this investigation include validation at higher Reynolds number conditions of the method used to treat the three-dimensional turbulent boundary layer, and the consideration of treating, for the three-dimensional case, the entire region between the body and the shock wave by a single set of equations which would be valid for both the viscous and inviscid flow regions. This latter treatment would implicitly include both the streamline-swallowing influences and boundary-layer displacement influences.

REFERENCES

1. Ferri, A. "Some Heat Transfer Problems in Hypersonic Flow." Aeronautics and Astronautics, Pergamon Press, New York, New York, 1960, pp. 344-377.

2. Mayne, A.W., Jr. and Adams, J.C., Jr. "Streamline Swallowing by Laminar Boundary Layers in Hypersonic Flow." AEDC-TR-71-32 (AD719748), March 1971.

3. Mayne, A.W., Jr. and Dyer, D.F. "Comparisons of Theory and Experiment for Turbulent Boundary Layers on Simple Shapes at Hypersonic Conditions." Proceedings of the 1970 Heat Transfer and Fluid Mechanics Institute, Stanford University Press, 1970, pp. 168-188.

4. Mayne, A.W., Jr. "Analysis of Laminar Boundary Layers on Right Circular Cones at Angle of Attack, Including Streamline-Swallowing Effects." AEDC-TR-72-134 (AD750130), October 1972.

5. Fannelop, T.K. and Waldman, G.D. "Displacement Interaction and Flow Separation on Cones at Incidence to a Hypersonic Stream." Paper No. 21 presented at the Advisory Group for Aerospace Research and Development Specialists' Meeting on "Hypersonic Boundary Layers and Flow Fields." London, England, May 1968.

6. Adams, J.C., Jr. "Implicit Finite-Difference Analysis of Compressible Laminar, Transitional, and Turbulent Boundary Layers Along the Windward Streamline of a Sharp Cone at Incidence." AEDC-TR-71-235 (AD734535), December 1971.

7. Mager, A. "Three-Dimensional Laminar Boundary Layers." High Speed Aerodynamics and Jet Propulsion, Vol. IV, Theory of Laminar Flows, F.K. Moore, Editor. Princeton, New Jersey, Princeton University Press, 1964, pp. 286-438.

8. Hunt, J.L., Bushnell, D.M., and Beckwith, I.E. "The Compressible Turbulent Boundary Layer on a Blunt Swept Slab with and without Leading-Edge Blowing." NASA TN D-6203, March 1971.

9. van Driest, E.R. "On Turbulent Flow Near a Wall." Journal of Aeronautical Sciences, Vol. 23, No. 11, November 1956, pp. 1007-1011, 1036.

10. Patankar, S.V. and Spalding, D.B. Heat and Mass Transfer in Boundary Layers, CRC Press, Cleveland, Ohio, 1968.

11. Dhawan, S. and Narasimha, R. "Some Properties of Boundary-Layer Flow during the Transition from Laminar to Turbulent Motion." Journal of Fluid Mechanics, Vol. 3, No. 4, April 1958, pp. 418-436.

12. Raetz, G.S. "A Method of Calculating Three-Dimensional Laminar Boundary Layers of Steady Compressible Flows." Northrop Aircraft Report NAI-58-73, Hawthorne, California, December 1957.

13. Der, J., Jr. and Raetz, G.S. "Solution of General Three-Dimensional Laminar Boundary-Layer Problems by an Exact Numerical Method." Institute of the Aerospace Sciences Paper No. 62-70, presented at the IAS Thirtieth Annual Meeting, New York, January 1962.

14. Wang, K.C. "On the Determination of the Zones of Influence and Dependence for Three-Dimensional Boundary-Layer Equations." Journal of Fluid Mechanics, Vol. 48, No. 2, 1971, pp. 397-404.

15. Rakich, J.V. "A Method of Characteristics for Steady Three-Dimensional Supersonic Flow with Application to Inclined Bodies of Revolution." NASA TN D-5341, October 1969.

16. Crank, J. and Nicholson, P. "A Practical Method for Numerical Evaluation of Solutions of Partial Differential Equations of the Heat-Conduction Type." Proceedings of the Cambridge Philosophical Society, Vol. 43, 1947, pp. 50-67.

17. Adams, J.C., Jr. "Higher Order Boundary-Layer Effects on Analytic Bodies of Revolution." AEDC-TR-68-57 (AD667523), April 1968.

18. Cleary, J.W. "Effects of Angle of Attack and Bluntness on Laminar Heating-Rate Distributions of a 15° Cone at a Mach Number of 10.6." NASA TN D-5450, October 1969.

19. Martellucci, A. and Neff, R.S. "The Influence of Asymmetric Transition on Reentry Vehicle Motion." AIAA Paper 70-987, presented at the AIAA Guidance, Control, and Flight Mechanics Conference, Santa Barbara, California, August 1970. See also Journal of Spacecraft and Rockets, Vol. 8, No. 5 May 1971, pp. 476-482.

UNCLASSIFIED
Security Classification

DOCUMENT CONTROL DATA - R & D

(Security classification of title, body of abstract and indexing annotation must be entered when the overall report is classified)

1. ORIGINATING ACTIVITY (Corporate author) Arnold Engineering Development Center Arnold Air Force Station, Tennessee 37389	2a. REPORT SECURITY CLASSIFICATION UNCLASSIFIED 2b. GROUP N/A

3. REPORT TITLE

CALCULATION OF THE BOUNDARY-LAYER FLOW IN THE WINDWARD SYMMETRY PLANE OF A SPHERICALLY BLUNTED AXISYMMETRIC BODY AT ANGLE OF ATTACK, INCLUDING STREAMLINE-SWALLOWING EFFECTS

4. DESCRIPTIVE NOTES (Type of report and inclusive dates)

Final Report - September 1971 to December 1972

5. AUTHOR(S) (First name, middle initial, last name)

Arloe W. Mayne, Jr., ARO, Inc.

6. REPORT DATE October 1973	7a. TOTAL NO. OF PAGES 53	7b. NO. OF REFS 19

8a. CONTRACT OR GRANT NO. b. PROJECT NO. c. Program Element 65802F d.	9a. ORIGINATOR'S REPORT NUMBER(S) AEDC-TR-73-166 9b. OTHER REPORT NO(S) (Any other numbers that may be assigned this report) ARO-VKF-TR-73-102

10. DISTRIBUTION STATEMENT

Approved for public release; distribution unlimited.

11. SUPPLEMENTARY NOTES Available in DDC	12. SPONSORING MILITARY ACTIVITY AEDC/AFSC Arnold AFS, Tennessee 37389

13. ABSTRACT The three-dimensional compressible boundary-layer equations are presented in a general Crocco-variables form, and particularized to the windward symmetry plane of a spherically blunted axisymmetric body at incidence under hypersonic conditions. Through the use of an eddy transport coefficient hypothesis and a streamwise intermittency factor, both transitional and fully turbulent boundary layers may be treated, in addition to laminar boundary-layer flow. A scheme is presented for determining the outer-edge boundary conditions to be applied to the boundary-layer equations, based on a mass flow balance treatment of the boundary-layer entrainment of the inviscid flow. A finite-difference technique is described for solving the set of partial differential equation governing the boundary-layer flow, and for treating the streamline-swallowing phenomenon. The method of treating the problem is validated by the good agreement obtained between results from the present method and both experimental data and other methods of calculation. Comparisons with experimental data are shown for both laminar and turbulent flow under hypersonic conditions and include cases where streamline-swallowing effects are large and cases where crossflow influences should be strong.

DD FORM 1 NOV 65 1473

UNCLASSIFIED
Security Classification

UNCLASSIFIED

Security Classification

14. KEY WORDS	LINK A ROLE	LINK A WT	LINK B ROLE	LINK B WT	LINK C ROLE	LINK C WT
computation						
boundary-layer flow						
symmetry plane (windward)						
spherically blunted						
axisymmetric body						
angle of attack						
hypersonic flow						

AFSC
Arnold AFS Tenn

UNCLASSIFIED

Security Classification